EUROPEAN ORGANIZATION FOR NUCLEAR RESEARCH

CERN–EP/99-174

16 December 1999

Measurement of the $\bar{\mathrm{B}} \to \mathrm{D}^{(*)}\pi\ell\bar{\nu}_\ell$ Branching Fraction

DELPHI Collaboration

Abstract

A study of b semileptonic decays into D, $D\pi^\pm$ and $D^*\pi^\pm$ final states is presented. The D^0, D^+ and D^{*+} mesons are exclusively reconstructed in Z decay data recorded from 1992 to 1995 in the DELPHI experiment at LEP. The overall branching fractions are measured to be:

$$\begin{aligned}
\mathrm{BR}(b \to D^0\ell^-\bar{\nu}_\ell X) &= (7.04 \pm 0.34\ (stat) \pm 0.36\ (syst.exp) \pm 0.17\ (\mathrm{BR}_D))\% \\
\mathrm{BR}(b \to D^+\ell^-\bar{\nu}_\ell X) &= (2.72 \pm 0.19\ (stat) \pm 0.16\ (syst.exp) \pm 0.18\ (\mathrm{BR}_D))\% \\
\mathrm{BR}(b \to D^{*+}\ell^-\bar{\nu}_\ell X) &= (2.75 \pm 0.17\ (stat) \pm 0.13\ (syst.exp) \pm 0.09\ (\mathrm{BR}_D))\%
\end{aligned}$$

where the D^0 and D^+ results include also contributions from D^{*0} and D^{*+} decays. A fit to the distribution of the $\pi^\pm$ impact parameter to the primary interaction vertex provides a measurement of the b semileptonic branching fractions into the $D^0\pi^\pm X$, $D^+\pi^\pm X$ and $D^{*+}\pi^\pm X$ final states. Assuming that single pion decay modes of B mesons dominate, the partial rates for $\bar{B} \to D\pi\ell^-\bar{\nu}_\ell$ and $\bar{B} \to D^*\pi\ell^-\bar{\nu}_\ell$ have been obtained, corresponding to a total branching fraction:

$$\mathrm{BR}(\bar{B} \to D\pi\ell^-\bar{\nu}_\ell) + \mathrm{BR}(\bar{B} \to D^*\pi\ell^-\bar{\nu}_\ell) = (3.40 \pm 0.52\ (stat) \pm 0.32\ (syst))\% \ .$$

This result agrees well with the observed difference between the total B semileptonic branching fraction and the sum of the $\bar{B} \to D\ell^-\bar{\nu}_\ell$ and $D^*\ell^-\bar{\nu}_\ell$ branching fractions.

(Phys. Lett. B475(2000)407)

P.Abreu[22], W.Adam[52], T.Adye[38], P.Adzic[12], I.Ajinenko[44], Z.Albrecht[18], T.Alderweireld[2], G.D.Alekseev[17], R.Alemany[51], T.Allmendinger[18], P.P.Allport[23], S.Almehed[25], U.Amaldi[9], N.Amapane[47], S.Amato[49], E.G.Anassontzis[3], P.Andersson[46], A.Andreazza[9], S.Andringa[22], P.Antilogus[26], W-D.Apel[18], Y.Arnoud[9], B.Åsman[46], J-E.Augustin[26], A.Augustinus[9], P.Baillon[9], P.Bambade[20], F.Barao[22], G.Barbiellini[48], R.Barbier[26], D.Y.Bardin[17], G.Barker[18], A.Baroncelli[40], M.Battaglia[16], M.Baubillier[24], K-H.Becks[54], M.Begalli[6], A.Behrmann[54], P.Beilliere[8], Yu.Belokopytov[9], N.C.Benekos[33], A.C.Benvenuti[5], C.Berat[15], M.Berggren[26], D.Bertini[26], D.Bertrand[2], M.Besancon[41], M.Bigi[47], M.S.Bilenky[17], M-A.Bizouard[20], D.Bloch[10], H.M.Blom[32], M.Bonesini[29], W.Bonivento[28], M.Boonekamp[41], P.S.L.Booth[23], A.W.Borgland[4], G.Borisov[20], C.Bosio[43], O.Botner[50], E.Boudinov[32], B.Bouquet[20], C.Bourdarios[20], T.J.V.Bowcock[23], I.Boyko[17], I.Bozovic[12], M.Bozzo[14], M.Bracko[45], P.Branchini[40], R.A.Brenner[50], P.Bruckman[9], J-M.Brunet[8], L.Bugge[34], T.Buran[34], B.Buschbeck[52], P.Buschmann[54], S.Cabrera[51], M.Caccia[28], M.Calvi[29], T.Camporesi[9], V.Canale[39], F.Carena[9], L.Carroll[23], C.Caso[14], M.V.Castillo Gimenez[51], A.Cattai[9], F.R.Cavallo[5], V.Chabaud[9], Ph.Charpentier[9], L.Chaussard[26], P.Checchia[37], G.A.Chelkov[17], R.Chierici[47], P.Chliapnikov[9,44], P.Chochula[7], V.Chorowicz[26], J.Chudoba[31], K.Cieslik[19], P.Collins[9], R.Contri[14], E.Cortina[51], G.Cosme[20], F.Cossutti[9], H.B.Crawley[1], D.Crennell[38], S.Crepe[15], G.Crosetti[14], J.Cuevas Maestro[35], S.Czellar[16], M.Davenport[9], W.Da Silva[24], G.Della Ricca[48], P.Delpierre[27], N.Demaria[9], A.De Angelis[48], W.De Boer[18], C.De Clercq[2], B.De Lotto[48], A.De Min[37], L.De Paula[49], H.Dijkstra[9], L.Di Ciaccio[9,39], J.Dolbeau[8], K.Doroba[53], M.Dracos[10], J.Drees[54], M.Dris[33], A.Duperrin[26], J-D.Durand[9], G.Eigen[4], T.Ekelof[50], G.Ekspong[46], M.Ellert[50], M.Elsing[9], J-P.Engel[10], M.Espirito Santo[22], G.Fanourakis[12], D.Fassouliotis[12], J.Fayot[24], M.Feindt[18], P.Ferrari[28], A.Ferrer[51], E.Ferrer-Ribas[20], F.Ferro[14], S.Fichet[24], A.Firestone[1], U.Flagmeyer[54], H.Foeth[9], E.Fokitis[33], F.Fontanelli[14], B.Franek[38], A.G.Frodesen[4], R.Fruhwirth[52], F.Fulda-Quenzer[20], J.Fuster[51], A.Galloni[23], D.Gamba[47], S.Gamblin[20], M.Gandelman[49], C.Garcia[51], C.Gaspar[9], M.Gaspar[49], U.Gasparini[37], Ph.Gavillet[9], E.N.Gazis[33], D.Gele[10], L.Gerdyukov[44], N.Ghodbane[26], I.Gil[51], F.Glege[54], R.Gokieli[9,53], B.Golob[9,45], G.Gomez-Ceballos[42], P.Goncalves[22], I.Gonzalez Caballero[42], G.Gopal[38], L.Gorn[1], V.Gracco[14], J.Grahl[1], E.Graziani[40], P.Gris[41], G.Grosdidier[20], K.Grzelak[53], J.Guy[38], F.Hahn[9], S.Hahn[54], S.Haider[9], A.Hallgren[50], K.Hamacher[54], J.Hansen[34], F.J.Harris[36], V.Hedberg[9,25], S.Heising[18], J.J.Hernandez[51], P.Herquet[2], H.Herr[9], T.L.Hessing[36], J.-M.Heuser[54], E.Higon[51], S-O.Holmgren[46], P.J.Holt[36], S.Hoorelbeke[2], M.Houlden[23], J.Hrubec[52], M.Huber[18], K.Huet[2], G.J.Hughes[23], K.Hultqvist[9,46], J.N.Jackson[23], R.Jacobsson[9], P.Jalocha[19], R.Janik[7], Ch.Jarlskog[25], G.Jarlskog[25], P.Jarry[41], B.Jean-Marie[20], D.Jeans[36], E.K.Johansson[46], P.Jonsson[26], C.Joram[9], P.Juillot[10], L.Jungermann[18], F.Kapusta[24], K.Karafasoulis[12], S.Katsanevas[26], E.C.Katsoufis[33], R.Keranen[18], G.Kernel[45], B.P.Kersevan[45], Yu.Khokhlov[44], B.A.Khomenko[17], N.N.Khovanski[17], A.Kiiskinen[16], B.King[23], A.Kinvig[23], N.J.Kjaer[9], O.Klapp[54], H.Klein[9], P.Kluit[32], P.Kokkinias[12], V.Kostioukhine[44], C.Kourkoumelis[3], O.Kouznetsov[41], M.Krammer[52], E.Kriznic[45], Z.Krumstein[17], P.Kubinec[7], J.Kurowska[53], K.Kurvinen[16], J.W.Lamsa[1], D.W.Lane[1], V.Lapin[44], J-P.Laugier[41], R.Lauhakangas[16], G.Leder[52], F.Ledroit[15], V.Lefebure[2], L.Leinonen[46], A.Leisos[12], R.Leitner[31], J.Lemonne[2], G.Lenzen[54], V.Lepeltier[20], T.Lesiak[19], M.Lethuillier[41], J.Libby[36], W.Liebig[54], D.Liko[9], A.Lipniacka[9,46], I.Lippi[37], B.Loerstad[25], J.G.Loken[36], J.H.Lopes[49], J.M.Lopez[42], R.Lopez-Fernandez[15], D.Loukas[12], P.Lutz[41], L.Lyons[36], J.MacNaughton[52], J.R.Mahon[6], A.Maio[22], A.Malek[54], T.G.M.Malmgren[46], S.Maltezos[33], V.Malychev[17], F.Mandl[52], J.Marco[42], R.Marco[42], B.Marechal[49], M.Margoni[37], J-C.Marin[9], C.Mariotti[9], A.Markou[12], C.Martinez-Rivero[20], F.Martinez-Vidal[51], S.Marti i Garcia[9], J.Masik[13], N.Mastroyiannopoulos[12], F.Matorras[42], C.Matteuzzi[29], G.Matthiae[39], F.Mazzucato[37], M.Mazzucato[37], M.Mc Cubbin[23], R.Mc Kay[1], R.Mc Nulty[23], G.Mc Pherson[23], C.Meroni[28], W.T.Meyer[1], A.Miagkov[44], E.Migliore[9], L.Mirabito[26], W.A.Mitaroff[52], U.Mjoernmark[25], T.Moa[46], M.Moch[18], R.Moeller[30], K.Moenig[9,11], M.R.Monge[14], X.Moreau[24], P.Morettini[14], G.Morton[36], U.Mueller[54], K.Muenich[54], M.Mulders[32], C.Mulet-Marquis[15], R.Muresan[25], W.J.Murray[38], B.Muryn[19], G.Myatt[36], T.Myklebust[34], F.Naraghi[15], M.Nassiakou[12], F.L.Navarria[5], S.Navas[51], K.Nawrocki[53], P.Negri[29], N.Neufeld[9], R.Nicolaidou[41], B.S.Nielsen[30], P.Niezurawski[53], M.Nikolenko[10,17], V.Nomokonov[16], A.Nygren[25], V.Obraztsov[44], A.G.Olshevski[17], A.Onofre[22], R.Orava[16], G.Orazi[10], K.Osterberg[16], A.Ouraou[41], M.Paganoni[29], S.Paiano[5], R.Pain[24], R.Paiva[22], J.Palacios[36], H.Palka[19], Th.D.Papadopoulou[9,33], K.Papageorgiou[12], L.Pape[9], C.Parkes[9], F.Parodi[14], U.Parzefall[23], A.Passeri[40], O.Passon[54], T.Pavel[25], M.Pegoraro[37], L.Peralta[22], M.Pernicka[52], A.Perrotta[5], C.Petridou[48], A.Petrolini[14], H.T.Phillips[38], F.Pierre[41], M.Pimenta[22], E.Piotto[28], T.Podobnik[45], M.E.Pol[6], G.Polok[19], P.Poropat[48], V.Pozdniakov[17], P.Privitera[39], N.Pukhaeva[17], A.Pullia[29], D.Radojicic[36], S.Ragazzi[29], H.Rahmani[33], J.Rames[13], P.N.Ratoff[21], A.L.Read[34], P.Rebecchi[9], N.G.Redaelli[28], M.Regler[52], J.Rehn[18], D.Reid[32], R.Reinhardt[54], P.B.Renton[36], L.K.Resvanis[3], F.Richard[20], J.Ridky[13], G.Rinaudo[47], I.Ripp-Baudot[10], O.Rohne[34], A.Romero[47], P.Ronchese[37], E.I.Rosenberg[1], P.Rosinsky[7], P.Roudeau[20], T.Rovelli[5], Ch.Royon[41], V.Ruhlmann-Kleider[41], A.Ruiz[42], H.Saarikko[16], Y.Sacquin[41], A.Sadovsky[17], G.Sajot[15], J.Salt[51], D.Sampsonidis[12], M.Sannino[14], Ph.Schwemling[24], B.Schwering[54], U.Schwickerath[18], F.Scuri[48], P.Seager[21], Y.Sedykh[17], A.M.Segar[36], N.Seibert[18], R.Sekulin[38], R.C.Shellard[6], M.Siebel[54], L.Simard[41], F.Simonetto[37], A.N.Sisakian[17], G.Smadja[26], N.Smirnov[44], O.Smirnova[25], G.R.Smith[38], A.Sokolov[44], A.Sopczak[18], R.Sosnowski[53], T.Spassov[22], E.Spiriti[40], S.Squarcia[14], C.Stanescu[40], S.Stanic[45], M.Stanitzki[18], K.Stevenson[36], A.Stocchi[20], J.Strauss[52], R.Strub[10], B.Stugu[4], M.Szczekowski[53], M.Szeptycka[53], T.Tabarelli[29], A.Taffard[23], F.Tegenfeldt[50], F.Terranova[29], J.Thomas[36], J.Timmermans[32], N.Tinti[5], L.G.Tkatchev[17], M.Tobin[23], S.Todorova[10], A.Tomaradze[2], B.Tome[22], A.Tonazzo[9], L.Tortora[40], P.Tortosa[51], G.Transtromer[25], D.Treille[9],

G.Tristram[8], M.Trochimczuk[53], C.Troncon[28], M-L.Turluer[41], I.A.Tyapkin[17], S.Tzamarias[12], O.Ullaland[9], V.Uvarov[44], G.Valenti[9,5], E.Vallazza[48], C.Vander Velde[2], P.Van Dam[32], W.Van den Boeck[2], W.K.Van Doninck[2], J.Van Eldik[9,32], A.Van Lysebetten[2], N.van Remortel[2], I.Van Vulpen[32], G.Vegni[28], L.Ventura[37], W.Venus[38,9], F.Verbeure[2], M.Verlato[37], L.S.Vertogradov[17], V.Verzi[39], D.Vilanova[41], L.Vitale[48], E.Vlasov[44], A.S.Vodopyanov[17], G.Voulgaris[3], V.Vrba[13], H.Wahlen[54], C.Walck[46], A.J.Washbrook[23], C.Weiser[9], D.Wicke[54], J.H.Wickens[2], G.R.Wilkinson[36], M.Winter[10], M.Witek[19], G.Wolf[9], J.Yi[1], O.Yushchenko[44], A.Zalewska[19], P.Zalewski[53], D.Zavrtanik[45], E.Zevgolatakos[12], N.I.Zimin[17,25], A.Zintchenko[17], Ph.Zoller[10], G.C.Zucchelli[46], G.Zumerle[37]

[1]Department of Physics and Astronomy, Iowa State University, Ames IA 50011-3160, USA
[2]Physics Department, Univ. Instelling Antwerpen, Universiteitsplein 1, B-2610 Antwerpen, Belgium
and IIHE, ULB-VUB, Pleinlaan 2, B-1050 Brussels, Belgium
and Faculté des Sciences, Univ. de l'Etat Mons, Av. Maistriau 19, B-7000 Mons, Belgium
[3]Physics Laboratory, University of Athens, Solonos Str. 104, GR-10680 Athens, Greece
[4]Department of Physics, University of Bergen, Allégaten 55, NO-5007 Bergen, Norway
[5]Dipartimento di Fisica, Università di Bologna and INFN, Via Irnerio 46, IT-40126 Bologna, Italy
[6]Centro Brasileiro de Pesquisas Físicas, rua Xavier Sigaud 150, BR-22290 Rio de Janeiro, Brazil
and Depto. de Física, Pont. Univ. Católica, C.P. 38071 BR-22453 Rio de Janeiro, Brazil
and Inst. de Física, Univ. Estadual do Rio de Janeiro, rua São Francisco Xavier 524, Rio de Janeiro, Brazil
[7]Comenius University, Faculty of Mathematics and Physics, Mlynska Dolina, SK-84215 Bratislava, Slovakia
[8]Collège de France, Lab. de Physique Corpusculaire, IN2P3-CNRS, FR-75231 Paris Cedex 05, France
[9]CERN, CH-1211 Geneva 23, Switzerland
[10]Institut de Recherches Subatomiques, IN2P3 - CNRS/ULP - BP20, FR-67037 Strasbourg Cedex, France
[11]Now at DESY-Zeuthen, Platanenallee 6, D-15735 Zeuthen, Germany
[12]Institute of Nuclear Physics, N.C.S.R. Demokritos, P.O. Box 60228, GR-15310 Athens, Greece
[13]FZU, Inst. of Phys. of the C.A.S. High Energy Physics Division, Na Slovance 2, CZ-180 40, Praha 8, Czech Republic
[14]Dipartimento di Fisica, Università di Genova and INFN, Via Dodecaneso 33, IT-16146 Genova, Italy
[15]Institut des Sciences Nucléaires, IN2P3-CNRS, Université de Grenoble 1, FR-38026 Grenoble Cedex, France
[16]Helsinki Institute of Physics, HIP, P.O. Box 9, FI-00014 Helsinki, Finland
[17]Joint Institute for Nuclear Research, Dubna, Head Post Office, P.O. Box 79, RU-101 000 Moscow, Russian Federation
[18]Institut für Experimentelle Kernphysik, Universität Karlsruhe, Postfach 6980, DE-76128 Karlsruhe, Germany
[19]Institute of Nuclear Physics and University of Mining and Metalurgy, Ul. Kawiory 26a, PL-30055 Krakow, Poland
[20]Université de Paris-Sud, Lab. de l'Accélérateur Linéaire, IN2P3-CNRS, Bât. 200, FR-91405 Orsay Cedex, France
[21]School of Physics and Chemistry, University of Lancaster, Lancaster LA1 4YB, UK
[22]LIP, IST, FCUL - Av. Elias Garcia, 14-1^{o}, PT-1000 Lisboa Codex, Portugal
[23]Department of Physics, University of Liverpool, P.O. Box 147, Liverpool L69 3BX, UK
[24]LPNHE, IN2P3-CNRS, Univ. Paris VI et VII, Tour 33 (RdC), 4 place Jussieu, FR-75252 Paris Cedex 05, France
[25]Department of Physics, University of Lund, Sölvegatan 14, SE-223 63 Lund, Sweden
[26]Université Claude Bernard de Lyon, IPNL, IN2P3-CNRS, FR-69622 Villeurbanne Cedex, France
[27]Univ. d'Aix - Marseille II - CPP, IN2P3-CNRS, FR-13288 Marseille Cedex 09, France
[28]Dipartimento di Fisica, Università di Milano and INFN, Via Celoria 16, IT-20133 Milan, Italy
[29]Università degli Studi di Milano - Bicocca, Via Emanuelli 15, IT-20126 Milan, Italy
[30]Niels Bohr Institute, Blegdamsvej 17, DK-2100 Copenhagen Ø, Denmark
[31]IPNP of MFF, Charles Univ., Areal MFF, V Holesovickach 2, CZ-180 00, Praha 8, Czech Republic
[32]NIKHEF, Postbus 41882, NL-1009 DB Amsterdam, The Netherlands
[33]National Technical University, Physics Department, Zografou Campus, GR-15773 Athens, Greece
[34]Physics Department, University of Oslo, Blindern, NO-1000 Oslo 3, Norway
[35]Dpto. Fisica, Univ. Oviedo, Avda. Calvo Sotelo s/n, ES-33007 Oviedo, Spain
[36]Department of Physics, University of Oxford, Keble Road, Oxford OX1 3RH, UK
[37]Dipartimento di Fisica, Università di Padova and INFN, Via Marzolo 8, IT-35131 Padua, Italy
[38]Rutherford Appleton Laboratory, Chilton, Didcot OX11 OQX, UK
[39]Dipartimento di Fisica, Università di Roma II and INFN, Tor Vergata, IT-00173 Rome, Italy
[40]Dipartimento di Fisica, Università di Roma III and INFN, Via della Vasca Navale 84, IT-00146 Rome, Italy
[41]DAPNIA/Service de Physique des Particules, CEA-Saclay, FR-91191 Gif-sur-Yvette Cedex, France
[42]Instituto de Fisica de Cantabria (CSIC-UC), Avda. los Castros s/n, ES-39006 Santander, Spain
[43]Dipartimento di Fisica, Università degli Studi di Roma La Sapienza, Piazzale Aldo Moro 2, IT-00185 Rome, Italy
[44]Inst. for High Energy Physics, Serpukov P.O. Box 35, Protvino, (Moscow Region), Russian Federation
[45]J. Stefan Institute, Jamova 39, SI-1000 Ljubljana, Slovenia and Laboratory for Astroparticle Physics,
Nova Gorica Polytechnic, Kostanjeviska 16a, SI-5000 Nova Gorica, Slovenia,
and Department of Physics, University of Ljubljana, SI-1000 Ljubljana, Slovenia
[46]Fysikum, Stockholm University, Box 6730, SE-113 85 Stockholm, Sweden
[47]Dipartimento di Fisica Sperimentale, Università di Torino and INFN, Via P. Giuria 1, IT-10125 Turin, Italy
[48]Dipartimento di Fisica, Università di Trieste and INFN, Via A. Valerio 2, IT-34127 Trieste, Italy
and Istituto di Fisica, Università di Udine, IT-33100 Udine, Italy
[49]Univ. Federal do Rio de Janeiro, C.P. 68528 Cidade Univ., Ilha do Fundão BR-21945-970 Rio de Janeiro, Brazil
[50]Department of Radiation Sciences, University of Uppsala, P.O. Box 535, SE-751 21 Uppsala, Sweden
[51]IFIC, Valencia-CSIC, and D.F.A.M.N., U. de Valencia, Avda. Dr. Moliner 50, ES-46100 Burjassot (Valencia), Spain
[52]Institut für Hochenergiephysik, Österr. Akad. d. Wissensch., Nikolsdorfergasse 18, AT-1050 Vienna, Austria
[53]Inst. Nuclear Studies and University of Warsaw, Ul. Hoza 69, PL-00681 Warsaw, Poland
[54]Fachbereich Physik, University of Wuppertal, Postfach 100 127, DE-42097 Wuppertal, Germany

1 Introduction

The study of $\bar{B}$ meson semileptonic decays into any $D\pi$ or $D^*\pi$ final state is interesting for several reasons. Present measurements of $\bar{B}$ semileptonic decays into $D\ell^-\bar{\nu}_\ell$ and $D^*\ell^-\bar{\nu}_\ell$ imply that these final states account for only 60% to 70% of all $\bar{B}$ semileptonic decays [1]. The remaining contribution could be attributed to the production of higher excited states or non-resonant $D^{(*)}\pi$ final states, hereafter denoted D^{**}. However the ALEPH measurement of the $D^{**}\ell^-\bar{\nu}_\ell$ branching fraction does not fully account for the observed discrepancy [2]. The ratio of branching fractions of $\bar{B}$ decays into $D^{*+}\pi^-\ell^-\bar{\nu}_\ell$ over all $D^{*+}\ell^-X$ final states [1] is also a significant contribution to the systematic uncertainty on $\tau_{B^0_d}$, Δm_d or V_{cb} measurements [1,3].

This paper describes a measurement of the branching fraction of $\bar{B} \to D^{**}\ell^-\bar{\nu}_\ell$ decays in the DELPHI experiment at LEP. The decays of the D^0, D^+ and D^{*+} into $D^0\pi^+_*$ are exclusively reconstructed [2]. The analysis of $D^{**} \to D^{(*)}\pi_{**}$ in $\bar{B}$ semileptonic decays [3] relies on the impact parameter of the π_{**} candidate, defined as its distance of closest approach to the reconstructed primary interaction vertex. A similar technique has been applied previously in ALEPH [4,2] and DELPHI [5]. The single pion final states $D^0\pi^+$, $D^+\pi^-$ or $D^{*+}\pi^-$, denoted "right" sign, are expected to dominate the decay widths. But pion pair emission, such as $D\pi^+\pi^-$, is also allowed and could provide "wrong" sign $D^0\pi^-$, $D^+\pi^+$ or $D^{*+}\pi^+$ combinations. Similarly D_s orbitally excited states can decay into D^0K^+ or $D^{*0}K^+$ which can be distinguished from $D^{(*)0}\pi^+$ if the kaon is identified.

The overall semileptonic branching fractions of a b quark into D^0, D^+ or D^{*+} final states are also presented in this paper.

2 The DELPHI detector

The DELPHI detector has been described in detail elsewhere [6,7]; only the detectors relevant to the present analysis are briefly described in the following. The tracking of charged particles is accomplished in the barrel region with a set of cylindrical tracking detectors whose axis is oriented along the 1.23 T magnetic field and the direction of the beam.

The Vertex Detector (VD) surrounds a Beryllium beam pipe with a radius of 5.5 cm. It consists of three concentric layers of silicon microstrip detectors at radii of 6, 9 and 11 cm from the beam line. In 1991-1993 all the VD layers were single-sided with strips parallel to the beam direction. In 1994 and 1995, the innermost and the outermost layers were replaced by double-sided silicon microstrip modules, providing a single hit precision of about 8 μm in $r\phi$, similar to that obtained previously, and between 10 μm and 20 μm in z [8] [4]. For polar angles between 44° and 136°, a track crosses all the three VD layers. The innermost layer covers the polar angle region between 25° and 155°. For charged particle tracks with hits in all three $r\phi$ VD layers, the impact parameter precision is [9]:

$$\sigma_{r\phi} = \frac{a}{p\sin^{3/2}\theta} \oplus b \qquad (1)$$

where $a = 61 \pm 1$ μm, $b = 20 \pm 1$ μm and p is the momentum in GeV/c.

[1] Throughout the paper charge-conjugate states are implicitly included; ℓ indicates an electron or a muon, not the sum over these two leptons.

[2] π_* denotes the charged pion from the $D^{*+} \to D^0\pi^+$ decay.

[3] D stands for D^0 or D^+; π_{**} denotes the charged pion from the decay of a higher excited state of charmed meson or from a non-resonant $D^{(*)}\pi$ final state.

[4] In the DELPHI coordinate system: z is along the beam line, ϕ is the azimuthal angle in the xy plane, transverse to the beam axis, r is the radius and θ is the polar angle with respect to the z axis.

The Inner Detector is placed outside the VD between radii of 12 cm and 28 cm. It consists of a jet chamber giving up to 24 spatial measurements and a trigger chamber providing a measurement of the z coordinate. The VD and ID are surrounded by the main DELPHI tracking chamber, the Time Projection Chamber (TPC), which provides up to 16 space points between radii of 30 cm and 122 cm. The Outer Detector (OD) at a radius of 198 cm to 206 cm consists of five layers of drift cells. The average momentum resolution of the tracking system is $\sigma(1/p) \ < \ 1.5 \times 10^{-3}$ (GeV/c)$^{-1}$ in the polar angle region between 25° and 155°. The tracking in the forward ($11° < \theta < 33°$) and backward ($147° < \theta < 169°$) regions is improved by two pairs of Forward drift Chambers (FCA and FCB) in the end-caps.

Hadrons were identified using the specific ionization (dE/dx) in the TPC and the Cherenkov radiation in the barrel Ring Imaging CHerenkov detector (RICH) placed between the TPC and the OD detectors.

The muon identification relied mainly on the muon chambers, a set of drift chambers giving three-dimensional information situated at the periphery of DELPHI after approximately 1 m of iron.

Electron identification relied mainly on the electromagnetic calorimeter in the barrel region (High density Projection Chamber HPC) which is a sampling device having a relative energy resolution of ±5.5% for electrons with 45.6 GeV/c momentum, and a spatial resolution along the beam axis of ±2 mm.

3 Event selection and simulation

Charged particles were required to have a measured momentum between 0.3 GeV/c and 50 GeV/c, a relative error on momentum less than 100%, a track length in the TPC larger than 30 cm and a distance of closest approach to the interaction point of less than 4 cm in r and less than 10 cm in z.

Hadronic events were required to have at least five charged particles with momentum greater than 0.4 GeV/c and a total energy of the charged particles (assumed to be pions) greater than 12% of the collision energy. A total of $N_Z = 3.51$ million hadronic events was obtained from the 1992-1995 data. Simulated hadronic events were generated using the JETSET 7.3 Parton Shower program [10]: 8.5 million $Z \to q\overline{q}$ and 4.0 million $Z \to b\overline{b}$ generated events, corresponding to seven times the available statistics in real data for $b\overline{b}$ final states. The B meson mean lifetime was set to $\tau_B^{\rm MC} = 1.6$ ps. The generated events were followed through a detailed detector simulation [7] and then processed through the same analysis chain as the real data. The hadronic event selection efficiency was thus estimated to be $\epsilon_Z = 95.7\%$. The data sample contained also 0.2% of τ pair events and 0.2% of Bhabha events.

The primary interaction vertex was computed in space for each event using an iterative procedure based on the χ^2 of the fit. The average transverse position of the interaction point, known for each fill, was included as a constraint during the primary vertex fit. In order to increase the $b\overline{b}$ purity of the selected sample, using the impact parameter of all measured charged particle tracks in the event, the probability that all these tracks originate from the primary vertex was required to be smaller than 0.1 [11]. This selection retains 15% of $Z \to u\bar{u}$, $d\bar{d}$ and $s\bar{s}$ events, 48% of $Z \to c\bar{c}$ events and 94% of $Z \to b\bar{b}$ events.

In order to estimate the reconstruction efficiencies and the invariant mass resolutions, dedicated samples of events containing a $\bar{B}$ meson decaying into $D^0\pi^+\ell^-\bar{\nu}_\ell X$, $D^+\pi^-\ell^-\bar{\nu}_\ell X$ or $D^{*+}\pi^-\ell^-\bar{\nu}_\ell X$ were generated. Physical backgrounds have also to be stud-

ied. These can be due to $b \to cW^-$ decays followed by $W^- \to \overline{c}s$ and $\overline{c} \to \ell^- \bar{\nu}_\ell X$ (hereafter denoted $b \to \overline{c} \to \ell$ background), or followed by $c \to \ell^+ \nu_\ell X$ with $W^- \to \bar{D}X$ (denoted $b \to c \to \overline{\ell}$ background). For this purpose, some dedicated samples of $\bar{B} \to D\bar{D}_s X$ or $D\bar{D}KX$ decays, with the $\bar{D}_s$ or $\bar{D}$ decaying semileptonically, were generated.

4 $D^{(*)}\ell^-$ selection

4.1 Lepton selection and identification

Both muon and electron candidates were selected with a momentum larger than 2 GeV/c. The lepton candidate was required to have at least one hit associated in the Vertex Detector.

The muon identification algorithm is described in reference [7]. A "loose" selection criterion provided an identification efficiency of $(90 \pm 2)\%$ for a probability of misidentifying a charged hadron as a muon of 1.2% within the acceptance of the muon chambers.

A neural network procedure, combining information from several detectors, has been developed for electron identification. Electrons were identified with an efficiency of $(65 \pm 2)\%$ and a misidentification probability that a hadron be identified as electron of about 0.4% [12].

The lepton transverse momentum relative to the $D^{(*)}$ meson momentum vector (as defined below) was required to be larger than 0.7 GeV/c. This cut reduced the contamination of leptons from b semileptonic decay into τ and from $b \to \overline{c} \to \ell$ or $b \to c \to \overline{\ell}$ decays.

4.2 $D^{(*)}$ decay channels

The $D^{(*)}$ meson candidates were reconstructed in the following decay channels: $D^0 \to K^-\pi^+$ or $K^-\pi^+\pi^+\pi^-$ (for D^0 not coming from a D^{*+} decay), $D^+ \to K^-\pi^+\pi^+$ and $D^{*+} \to D^0\pi_*^+$ with a D^0 decaying into $K^-\pi^+$, $K^-\pi^+\pi^+\pi^-$ or $K^-\pi^+(\pi^0)$ where the π^0 was not reconstructed. In order to optimize the statistical precision of the measured production rates, slightly different selection criteria, as described below, were chosen in each $D^{(*)}$ meson sample.

Only charged particles with momentum vectors in the hemisphere defined by the lepton direction were considered for the reconstruction of charmed mesons. The kaon candidate from the D decay was required to have the same charge as the identified lepton. The kaon momentum was required to be larger than 1 (2) GeV/c in the D^0 (D^+) channel. The momentum of each pion from the $D^{0/+}$ decay had to be larger than 1 GeV/c, except for the $K^-\pi^+\pi^+\pi^-$ final state where the minimum momentum of candidate pions was lowered to 0.5 (0.3) GeV/c in the D^0 (D^{*+}) analysis. Any charged particle with a momentum between 0.3 GeV/c and 4.5 GeV/c and a charge opposite to that of the kaon was used as pion candidate for the $D^{*+} \to D^0\pi_*^+$ decay channel.

To reduce the combinatorial background for all channels, except in the $D^{*+} \to (K^-\pi^+)\pi_*^+$ decay, the kaon candidate of the D was required to be identified according to the RICH and dE/dx information [7]. In the $D^0 \to K^-\pi^+$ and $D^0 \to K^-\pi^+(\pi^0)$ decay channels, the angle θ^* between the $K^-\pi^+$ momentum vector and the kaon direction in the $K^-\pi^+$ rest frame was required to satisfy the condition $\cos\theta^* > -0.8$. For genuine D^0 candidates an isotropic distribution in $\cos\theta^*$ is expected whereas the background is strongly peaked in the backward direction.

The π_* candidate and at least two particles from the $D^{0/+}$ decay were required to have at least one hit associated in the Vertex Detector.

4.3 D vertex

After the previous selections, a $K^-\pi^+$, $K^-\pi^+\pi^+$ or $K^-\pi^+\pi^+\pi^-$ vertex was fitted in space. In the $K^-\pi^+\pi^+\pi^-$ decay channel, in order to reduce the large combinatorial background, the impact parameters of charged particle trajectories, relative to the common D^0 vertex, were required to be smaller than 150 μm. In the $D^+ \to K^-\pi^+\pi^+$ channel, either these impact parameters had to be less than 100 μm or the χ^2 probability of the $K^-\pi^+\pi^+$ vertex had to be larger than 10^{-4}.

The momentum vector of each particle, attached to the D vertex, was recomputed at this vertex. In each channel, the scaled D energy, $X_E(D) = E(D)/E_{\rm beam}$, was required to be larger than 0.15.

The apparent decay length of the D^0 or D^+ candidate, ΔL, was computed in the plane transverse to the beam axis. It was given the same sign as the scalar product of the D momentum direction with the vector joining the primary to the D vertices. In the D^{*+} channel, ΔL was required to be positive. In the D^0 and D^+ channels, which have a higher combinatorial background, the value of ΔL divided by its error was required to be larger than 1.

4.4 B vertex

Finally a $D^0\ell$, $D^+\ell$ or $D^0\pi_*\ell$ vertex (denoted "B" vertex in the following) was fitted in space. The B decay length was defined, as above, as the signed distance between the primary vertex and the secondary $D(\pi_*)\ell$ vertex in the plane transverse to the beam axis. This B decay length divided by its error was required to be larger than 1 for all channels. In order to reduce further the combinatorial background, the decay length divided by its error between the D and the B vertices was also computed: it was required to be larger than -1 in the D^0 samples and in the $D^{*+} \to (K^-\pi^+\pi^+\pi^-)\pi^+_*$ sample, and to be positive in the D^+ sample.

4.5 D invariant mass

The selection of $D^{*+}\ell^-$ events relied on the small mass difference (ΔM) between the D^{*+} and the candidate D^0. On the contrary, D^{*+} candidates were rejected from the D^0 and D^+ samples as follows: the D^0 candidates were rejected if at least one π_* particle was found in the event giving a ΔM value less than 160 MeV/c^2; in the $D^+ \to K^-\pi^+\pi^+$ sample, both $K^-\pi^+$ pairs were associated to the remaining π^+ and a ΔM mass difference was computed, the $K^-\pi^+\pi^+$ combination was rejected if at least one ΔM value was found smaller than 160 MeV/c^2.

Figure 1 shows the invariant mass (or mass difference) distributions in each of the previously selected D meson channels. In the $D^{*+} \to (K^-\pi^+)\pi^+_*$ channel, the $K^-\pi^+$ invariant mass had to be within 75 MeV/c^2 of the nominal D^0 mass. In the $D^{*+} \to (K^-\pi^+(\pi^0))\pi^+_*$ channel, the $K^-\pi^+$ invariant mass had to be between 1500 and 1700 MeV/c^2. In the $D^{*+} \to (K^-\pi^+\pi^+\pi^-)\pi^+_*$ channel, the ΔM mass difference had to be within 2 MeV/c^2 of the nominal $D^{*+} - D^0$ mass difference. The invariant mass of the $D^0 \to K^-\pi^+$ channel has a resolution of about 25 MeV/c^2 whereas it is less than 15 MeV/c^2 in the $K^-\pi^+\pi^+\pi^-$ final state. Thus, in the particular case of the $D^{*+} \to (K^-\pi^+)\pi^+_*$ decay channel, the $K^-\pi^+$ invariant mass was constrained to the D^0 mass value and a constrained $(D^0\pi_*\ell)$ kinematic fit was performed. This improved the resolution of the $(D^{*+} - D^0)$ mass difference by 30% in this channel.

A clear signal corresponding to $D\ell^-$ events is observed in each distribution (data points), whereas the wrong sign $D\ell^+$ combinations (hatched histograms) present a much smaller D meson contribution. The right sign invariant mass distributions were fitted with a signal component described by the sum of Gaussian functions, and a combinatorial background parameterised with a polynomial form. In the $D^0 \to K\pi$ and $K\pi\pi\pi$ samples, the contribution from missing π^0 appears as a "satellite" peak for mass values smaller than the nominal D^0 mass. This contribution was parameterised as the sum of Gaussian functions with their parameters fixed according to the simulation. In each channel, the relative amounts and relative widths of the Gaussian functions describing the D signal were tuned according to the simulation. The free parameters of the fits were thus the coefficients of the polynomial background, the normalisation of the "satellite" peak (in the $K\pi$ and $K\pi\pi\pi$ invariant mass distributions), the average width and mean value of the signal shape and the number of D signal candidates. For each decay channel, the mass distributions of the wrong sign $D\ell^+$ events were fitted with the same shape parameters as the right sign signals. This allowed the contribution of the fake lepton events to be determined and then subtracted. The observed numbers of D mesons, within the quoted range around the $D^{0/+}$ mass and $D^{*+} - D^0$ mass difference, is indicated in Table 1.

	Mass range (MeV/c^2)		Nb. of	Nb. of
D sample	$M(D^{0/+})$	ΔM	$D\ell^-$	$D\ell^+$
$D^0 \to K^-\pi^+$	1820-1910	>160	752±41	6±18
$D^0 \to K^-\pi^+\pi^+\pi^-$	1840-1890	>160	689±43	39±26
$D^+ \to K^-\pi^+\pi^+$	1830-1910	>160	763±44	66±19
$D^{*+} \to (K^-\pi^+)\pi^+_*$	1790-1940	143.5-147.5	416±24	18±5
$D^{*+} \to (K^-\pi^+\pi^+\pi^-)\pi^+_*$	1840-1890	143.5-147.5	303±21	5±5
$D^{*+} \to (K^-\pi^+(\pi^0))\pi^+_*$	1500-1700	<155	522±33	15±12

Table 1: Mass selections and number of D candidates observed in each decay channel (with their statistical error). Note that most of the $D^{*+} \to D^0\pi^+_*$ candidates were removed from the selected D^0 sample; the D^+ sample also includes $D^{*+} \to D^+\pi^0$ (or γ) decays.

5 Semileptonic b decay rate into $D\pi\ell^-X$ or $D^*\pi\ell^-X$

In this section, a search for any $D\pi_{**}$ final state is described, based on the impact parameter distribution of the π_{**} candidates relative to the primary interaction vertex and using the D decay channels selected in the previous section.

5.1 $D^{**}\ell^-$ selection

The selection criteria for the additional π_{**} candidate were identical for all decay channels. All charged particles with a momentum greater than 0.5 GeV/c and produced in the hemisphere defined by the $D(\pi_*)\ell^-$ momentum vector were considered as π_{**} candidates. The invariant $D(\pi_*)\pi_{**}\ell$ mass had to be smaller than 5.5 GeV/c^2. The π_{**} track was required to have at least 2 hits in the Vertex Detector. Its combined RICH and dE/dx information had not to be compatible with the kaon hypothesis. The impact parameter

of this π_{**} relative to the previously fitted $D(\pi_*)\ell$ vertex was required to be smaller than 100 μm.

For each π_{**} candidate, the impact parameter relative to the primary interaction vertex was computed in the plane transverse to the beam axis. The sign of this impact parameter was defined with respect to the $D(\pi_*)\ell$ direction. It was positive if the intercept between the π_{**} and the $D(\pi_*)\ell$ momentum vectors was downstream of the primary vertex along the $D(\pi_*)\ell$ direction, and negative if it was upstream [11].

The π_{**} impact parameter distribution of simulated B semileptonic decays is shown in Figure 2a. Compared with charged particles produced in b quark fragmentation or gluon radiation in jets (see Figure 2b), π_{**} from $\bar{B} \to D^{**}\ell^-\bar{\nu}_\ell$ decays present a tail at large positive impact parameters due to the long B lifetime.

5.2 Backgrounds

For real data $D^{**}\ell$ candidates, two sources of background had to be subtracted:

- Fake D associated to a lepton candidate: this combinatorial background was estimated by using events in the tails of the mass distributions of Figure 1, after a normalisation to the fraction of events below the D signals. Figures 3a-c present the impact parameter distributions of all pion candidates associated to a fake D (points with error bars) and to a D in the tails of the mass distributions (histograms) from the D samples selected in the $q\overline{q}$ simulation. A good agreement is found between the true background and the mass tail estimate.
- True D associated to a fake lepton: this background is due to charged pions and kaons misidentified as leptons. It has been subtracted by using the π_{**} candidates produced in the same direction as a wrong sign $D\ell^+$ event (shown in the hatched histograms of Figure 1) where the D candidate was selected in the mass range defined in Table 1. Figure 3d presents the impact parameter distributions of all pion candidates associated to a fake lepton (points with error bars) and to a $D\ell^+$ event (histograms) from the D samples selected in the $q\overline{q}$ simulation. Here also a good agreement is found between the true background and the ℓ^+ estimate.

In the real data events, the same procedure was applied. The shapes of these backgrounds were taken from the real data themselves and their normalisation was estimated according to the fit of the mass distributions of Figure 1.

After the subtraction of these backgrounds, all the remaining pions can be attributed to b decays into $D\pi\ell^-X$ final state. However, four kinds of pions are still to be considered:

- genuine π_{**} from $\bar{B} \to D^{**}\ell^-\bar{\nu}_\ell$ decays (see Figure 2a);
- particles from jet fragmentation (see Figure 2b);
- "$\tau, c \to \ell$" background: it includes pions produced in D^{**} decays when the D^{**} is not issued from a direct semileptonic (e or μ) b decay. This D^{**} can be produced in $b \to D^{**}\tau^-\bar{\nu}_\tau$ decay, or in $b \to D^{**}\bar{D}_{(s)}X$ (or $b \to D\bar{D}^{**}X$) transitions, when the other $\bar{D}_{(s)}$ (or D) meson decays semileptonically;
- "hadronic" background: it is due to other hadrons, denoted H, produced from the $\overline{c}$ in $b \to \overline{c} \to \ell$ decay events or from the c in $b \to c \to \overline{\ell}$ (when the other charm quark fragments into a D meson). Such hadrons can be also emitted directly from the $\bar{B}$ meson.

Despite the momentum and transverse momentum cuts applied to the lepton, these last two classes were not fully eliminated. Their impact parameter distributions were similar

to the impact parameter distribution of genuine π_{**} from b semileptonic decays. These two last backgrounds were thus fitted together with the genuine π_{**} signal and subtracted only afterwards. Measured results were used for their rates and their selection efficiencies were obtained from the simulation (see Section 5.4.3).

5.3 Total yield

In the real data, the impact parameter distributions of the π_{**} candidates of the "right" sign $D^0\pi^+\ell^-$, $D^+\pi^-\ell^-$ and $D^{*+}\pi^-\ell^-$ samples are shown in Figure 4. They were fitted, fixing the fake D and fake lepton backgrounds, but letting free the normalisation of the fragmentation and π_{**} components. Figure 5 shows the same distributions, after subtraction of the fake D and fake lepton backgrounds. Similar fits were performed to the "wrong" sign $D^0\pi^-\ell^-$, $D^+\pi^+\ell^-$ and $D^{*+}\pi^+\ell^-$ samples and are shown in Figure 6 after the subtraction of the fake D and fake lepton backgrounds.

Instead of rejecting kaons in order to select π_{**} , kaons were also identified in order to select K_{**} from $D_{s1} \to D^{*0}K^+$, $D^*_{s2} \to D^0K^+$ decays or any other D^0K^+X final state from other D_{sJ} resonances. The corresponding impact parameter distributions are shown in the same figures as above. The kaon rejection requirement led to a π_{**} identification efficiency of $(92 \pm 1)\%$ and a probability of wrong assignment as a kaon of $(8 \pm 1)\%$. The kaon identification requirement lead to a K_{**} identification efficiency of $(60 \pm 2)\%$ and a probability of wrong assignment as a pion of $(40 \pm 2)\%$. These factors were obtained from the real data, as explained in Section 5.4.1 ($f_{\pi\text{id}}$ correction). The numbers of fitted $D^0\pi\ell^-$ and $D^0K\ell^-$ were $163 \pm 34(stat)$ and $39 \pm 15(stat)$ ($48 \pm 21(stat)$ and $5 \pm 8(stat)$) in the "right" sign ("wrong" sign) samples. These values need to be corrected in order to take into account the fraction of kaons misidentified as pions.

The final amounts, $N(D\pi\ell^-)$, of "right" and "wrong" signs fitted candidates are presented in Table 2 for all considered channels. In the D^0 channel, the separated contributions of $D^0\pi$, D^0K and the total D^0h are also indicated (where "h" means that the π_{**} candidate was selected without identification). Significant numbers of "right" sign candidates are fitted for all channels, whereas the number of "wrong" signs are clearly smaller.

5.4 $D^{**}\ell^-$ efficiency

The semileptonic branching fraction of a b quark into $D\pi$ final state was then measured as follows:

$$\mathrm{BR}(b \to D\pi\ell^- X) = \frac{\epsilon_Z}{N_Z}\,\frac{1}{2R_b}\,\frac{N(D\pi\ell^-)}{2\,\epsilon_{D\ell}\,\epsilon_{**}}\,\frac{f_{\tau_B}}{f_{\mathrm{cor}}}\,\frac{1-f_{\tau,c\to\ell}}{\mathrm{BR}_D}\;-\;\mathcal{F}_H\;-\;\mathcal{F}_{D^*} \qquad (2)$$

where N_Z and ϵ_Z are defined in Section 3, $R_b = 0.2166 \pm 0.0007$ is the Z hadronic decay rate into $b\overline{b}$ events [13]; the branching fractions, BR_D, in the three decay modes $\mathrm{BR}(D^0 \to K^-\pi^+) = 0.0385 \pm 0.0009$, $\mathrm{BR}(D^+ \to K^-\pi^+\pi^+) = 0.090 \pm 0.006$ and $\mathrm{BR}(D^{*+} \to D^0\pi^+_*) = 0.683 \pm 0.014$ are used [1]. The efficiencies to reconstruct and select the $D\ell^-$ and π_{**} (or K_{**}) candidates from $\bar{B} \to D^{**}\ell^-\bar{\nu}_\ell$ decays, denoted $\epsilon_{D\ell}$ and ϵ_{**} respectively, are indicated in Table 2. They were obtained from the simulation and corrected by the factors f_{cor} and f_{τ_B} which are described below. The correction factors $f_{\tau,c\to\ell}$ and $\mathcal{F}_H$ account for the "$\tau, c \to \ell$" and "hadronic" backgrounds introduced in Section 5.2; $\mathcal{F}_{D^*}$ is the background due to residual $D^{*+}\pi^-\ell^-$ which applies to the "wrong" sign $D^0\pi^-\ell^-$ and $D^0K^-\ell^-$ samples only.

Sample	$D^0h\ell^-$	$D^0\pi\ell^-$	$D^0K\ell^-$	$D^+\pi\ell^-$	$D^{*+}\pi\ell^-$
N("right" sign)	202 ± 37	182 ± 39	20 ± 18	75 ± 25	132 ± 22
N("wrong" sign)	53 ± 23	55 ± 24	-2 ± 10	41 ± 20	24 ± 16
$\epsilon_{D\ell}$	0.127 ± 0.002			0.095 ± 0.002	0.150 ± 0.002
ϵ_{**}	0.655 ± 0.006			0.649 ± 0.008	0.654 ± 0.005
$f_{K\pi}$	1.87 ± 0.09			1	3.02 ± 0.16
f_{M_D}	0.94 ± 0.01			0.98 ± 0.01	1.01 ± 0.01
$f_{\rm VD}$	1.00 ± 0.03			1.00 ± 0.03	1.00 ± 0.03
$f_{D\rm vtx}$	1			0.97 ± 0.03	1
$f_{K\rm id}$	0.84 ± 0.02			0.83 ± 0.02	1
$f_{\pi\rm id}$	1			0.92 ± 0.01	0.92 ± 0.01
f_{τ_B}("right" sign)	1.02 ± 0.02			0.98 ± 0.02	0.98 ± 0.01
f_{τ_B}("wrong" sign)	0.98 ± 0.02			1.02 ± 0.02	1.03 ± 0.03
$f_{\tau,c\to\ell}$	0.075 ± 0.030			0.075 ± 0.030	0.075 ± 0.030
$\mathcal{F}_H$ ($\times 10^{-3}$)	1.06 ± 0.29	0.78 ± 0.22	0.28 ± 0.09	0.40 ± 0.12	0.41 ± 0.11
$\mathcal{F}_{D^*}$ ($\times 10^{-3}$)	0.25 ± 0.06	0.23 ± 0.06	0.02 ± 0.01	0	0

Table 2: Number of fitted $D\pi\ell^-$ candidates; reconstruction times selection efficiencies of the $D\ell^-$ and π_{**} (or K_{**}) from $\bar{B} \to D^{**}\ell^-\bar{\nu}_\ell$ decays; correction factors introduced in equation (2). Errors are statistical only (except for $f_{\tau,c\to\ell}$ and $\mathcal{F}_H$). Note that most of the $D^{*+} \to D^0\pi^+_*$ candidates have been removed from the selected D^0 sample; the D^0 sample also includes $D^{*0} \to D^0\pi^0$ (or γ) decays; the D^+ sample also includes $D^{*+} \to D^+\pi^0$ (or γ) decays.

5.4.1 Efficiency correction

The correction to the reconstruction and selection efficiency is expressed as $f_{\rm cor} = f_{K\pi}\ f_{M_D}\ f_{\rm VD}\ f_{D\rm vtx}\ f_{K\rm id}\ f_{\pi\rm id}$:

- In the $D^0\ell$ and $D^{*+}\ell$ samples, only the $K\pi$ decay channel was used to estimate the $\epsilon_{D\ell}$ efficiency. For these samples, $f_{K\pi} = N(D\ell)/N(D_{K\pi}\ell)$ where $N(D\ell) = N(D\ell^-) - N(D\ell^+)$ is the difference between the total number of $D\ell$ candidates quoted in Table 1 and $N(D_{K\pi}\ell)$ is the same difference computed in the $K\pi$ decay mode only of the D^0. In the $D^+\ell$ sample, $f_{K\pi} = 1$.
- Due to the D mass ranges required in Table 1, f_{M_D} accounts for the mass width differences observed in real data and simulation.
- A large sample of $D^{*+} \to (K^-\pi^+)\pi^+_*$ reconstructed inside b-tagged jets was used in order to estimate selection efficiencies related to the detector response: the Vertex Detector information which was required for all channels ($f_{\rm VD}$ factor), the vertex quality cuts for the D^+ sample ($f_{D\rm vtx}$), and the kaon identification for the D^0 and D^+ samples ($f_{K\rm id}$). For the study of the $K^-\pi^+\pi^+$ vertex quality in the D^+ sample, a three tracks $K^-\pi^+\pi^+_*$ vertex was also fitted in the dedicated D^{*+} sample and similar cuts were applied.
- The kaon rejection (or identification) requirement of the π_{**} (K_{**}) candidates was also checked on the same dedicated D^{*+} sample and a correction factor $f_{\pi\rm id}$ was inferred.

5.4.2 B lifetime correction

The difference between the known values of the B mesons' mean lifetimes ($\tau_{B^+} = 1.65 \pm 0.04$ ps, $\tau_{B^0} = 1.56 \pm 0.04$ ps [17], $\tau_{B_s}/\tau_{B^0} \sim 0.99 - 1.01$ [18]) and that used in the Monte Carlo simulation ($\tau_B^{\rm MC} = 1.6$ ps) has two consequences:

- It affects the decay length selection efficiencies described in Section 4. But as these selections were applied to the decay lengths divided by their errors, the relative correction to $\epsilon_{D\ell}$ was found to be of about $\pm 0.2\%$ only. It was thus included in the following f_{τ_B} factor.
- It also affects the shape of the impact parameter distribution of simulated π_{**} candidates which is used to fit the amount of $D\pi\ell^-$ candidates in real data. The distribution shown in Figure 2a was thus recomputed by weighting each simulated event and by using the B^0 mean lifetime for "right" sign $D^0 h^+ \ell^-$ and "wrong" sign $D^{(*)+}\pi^+\ell^-$ candidates, or the B^+ mean lifetime for "right" sign $D^{(*)+}\pi^-\ell^-$ and "wrong" sign $D^0 h^-\ell^-$. These new π_{**} impact parameter shapes were used to fit the real data distributions shown in Figures 4-6. The difference between the number of fitted $D^{(*)}\pi_{**}\ell X$ candidates observed with and without the weighting procedure is described by the correction factor, f_{τ_B}, given in Table 2.

5.4.3 Physical background correction

The physical background contributions are determined in the following way:

- According to the simulation, still $(7.6 \pm 0.4\ (stat))\%$ of $D^{*+} \to D^0\pi_*^+$ remained in the D^0 sample; this value was used to determine the $\mathcal{F}_{D^*}$ factor.
- The fraction of $b \to \tau \to \ell$ events is evaluated as:

$$f_{\tau\to\ell} = \frac{\mathrm{BR}(b \to \tau^-\bar\nu_\tau X)\mathrm{BR}(\tau^- \to \ell^-\bar\nu_\ell\nu_\tau)}{\mathrm{BR}(b \to \ell^-\bar\nu_\ell X)}\ \frac{\epsilon_{\tau\to\ell}}{\epsilon_\ell} = 0.0075 \pm 0.0020 \qquad (3)$$

  where $\mathrm{BR}(b \to \tau^-\bar\nu_\tau X) = (2.6 \pm 0.4)\%$, $\mathrm{BR}(\tau^- \to \ell^-\bar\nu_\ell\nu_\tau) = (17.64 \pm 0.06)\%$ and $\mathrm{BR}(b \to \ell^-\bar\nu_\ell X) = (10.99 \pm 0.23)\%$ [1]; $\epsilon_{\tau\to\ell}/\epsilon_\ell = 0.18 \pm 0.04\ (stat)$ is the ratio of the lepton selection efficiencies in $b \to \tau^-\bar\nu_\tau X$ and $b \to \ell^-\bar\nu_\ell X$ simulated events.
  The fraction of $b \to \overline{c} \to \ell$ events is evaluated as:

$$f_{\overline{c}\to\ell} = \frac{\mathrm{BR}(b \to \overline{c} \to \ell)}{\mathrm{BR}(b \to \ell^-\bar\nu_\ell X)}\ \frac{\epsilon_{c\to\ell}}{\epsilon_\ell} = 0.047 \pm 0.012 \qquad (4)$$

  where $\mathrm{BR}(b \to \overline{c} \to \ell)) = (1.6 \pm 0.4)\%$ [14]; $\epsilon_{c\to\ell}/\epsilon_\ell = 0.32 \pm 0.02\ (stat)$ is the ratio of the lepton selection efficiencies in $b \to \overline{c} \to \ell$ and $b \to \ell^-\bar\nu_\ell X$ simulated events.
  The fraction of $b \to c \to \overline{\ell}$ events is obtained as previously, but the probability, $P_{W\to D}$, for the virtual W^- to decay into a $\overline{D}^0$ or D^- meson has to be taken into account:

$$f_{c\to\ell} = \frac{\mathrm{BR}(b \to c \to \overline{\ell})}{\mathrm{BR}(b \to \ell^-\bar\nu_\ell X)}\ P_{W\to D}\ \frac{\epsilon_{c\to\ell}}{\epsilon_\ell} = 0.020 \pm 0.005 \qquad (5)$$

  where $\mathrm{BR}(b \to c \to \overline{\ell}) = (7.8 \pm 0.6)\%$ [1] and $P_{W\to D} = (9.0 \pm 1.9)\%$ [14]. Finally the fraction of D^{**} not issued from a direct semileptonic b decay is evaluated to be:

$$f_{\tau,c\to\ell} = f_{\tau\to\ell} + f_{\overline{c}\to\ell} + f_{c\to\ell} = 0.075 \pm 0.017 \pm 0.025\ . \qquad (6)$$

  In the first error, which is the sum of the uncertainties quoted in equations (3-5), the errors on $f_{\overline{c}\to\ell}$ and $f_{c\to\ell}$ have been added linearly because $P_{W\to D}$ was used in

reference [14] to evaluate $\mathrm{BR}(b \to \overline{c} \to \ell)$. The second error in equation (6) is an estimate of the uncertainty due to possible phase space or QCD corrections between the $b \to \ell$ and the $b \to \tau, c \to \ell$ decay channels with a D^{**} in the final state.

- The "hadronic" background is evaluated as:

$$\mathcal{F}_H = \mathrm{BR}(b \to DX)\,(1 - P_{W\to D})\,\mathrm{BR}(b \to (c \text{ or } \overline{c}) \to \ell^{\pm})\,\frac{\epsilon_{b\to DH\ell X}}{\epsilon_{D\ell}\epsilon_{**}} \qquad (7)$$

with

$$\begin{aligned}\mathrm{BR}(b \to (c \text{ or } \overline{c}) \to \ell^{\pm}) &= \mathrm{BR}(b \to \overline{c} \to \ell) + \mathrm{BR}(b \to c \to \overline{\ell})\,P_{W\to D} \\ &= (2.30 \pm 0.56)\%\,, \qquad (8)\end{aligned}$$

$\mathrm{BR}(b \to D^0X) = (60.1 \pm 3.2)\%$ [1], $\mathrm{BR}(b \to D^+X) = (23.0 \pm 2.1)\%$ and $\mathrm{BR}(b \to D^{*+}X) = (23.1 \pm 1.3)\%$ [15]; the difference $\mathrm{BR}(b \to D^0X) - \mathrm{BR}(b \to D^{*+}X)\mathrm{BR}(D^{*+} \to D^0\pi^+) = (44.3 \pm 3.3)\%$ is used for the $D^0\ell^-$ analysis, where the D^{*+} were rejected. In the $D\pi\ell^-$ analyses, $\epsilon_{b\to DH\ell X}/(\epsilon_{D\ell}\epsilon_{**}) = 0.084 \pm 0.010\ (stat)$ was determined from the simulation as the ratio of selection efficiencies between hadrons from charm decay in $b \to \overline{c} \to \ell$ events, and genuine π_{**} in $\bar{B} \to D^{**}\ell^-\bar{\nu}_\ell$ decay; in the $D^0K\ell^-$ analysis, this ratio was estimated to be $0.030 \pm 0.006\ (stat)$. The resulting $\mathcal{F}_H$ values are reported in Table 2.

5.5 Systematics

The systematics are detailed in Table 3. As a cross-check of the procedure, the same analysis was repeated on simulated $q\overline{q}$ and $b\overline{b}$ samples:

- 1998 ± 107 (1017 ± 73, 870 ± 62) D^{**} candidates were fitted in the "right" sign $D^0\pi^+\ell^-$ ($D^+\pi^-\ell^-$, $D^{*+}\pi^-\ell^-$) samples whereas 1934 (1106, 879) D^{**} were expected;
- 396 ± 67 (219 ± 52, 60 ± 38) D^{**} candidates were fitted in the "wrong" sign $D^0\pi^+\ell^-$ ($D^+\pi^-\ell^-$, $D^{*+}\pi^-\ell^-$) samples whereas 333 (235, 62) D^{**} were expected.

A good agreement was thus obtained in the simulation between the fitted and expected π_{**} contributions, the related statistical error being used to estimate the systematic uncertainty due to the subtraction of the fake D and fake lepton backgrounds. The remaining statistical error of the Monte Carlo simulation is due to the limited number of generated $\bar{B} \to D\pi\ell^-\bar{\nu}_\ell X$ events.

Following the detailed study of reference [16], a $\pm 0.3\%$ uncertainty is assigned to the reconstruction efficiency of each charged particle.

The uncertainty on the impact parameter resolution has two sources:

- Impact parameter relative to the primary interaction vertex:
  the uncertainty on the parameters a and b of equation (1) affects the impact parameter distributions of Figure 2 and thus the result of the fit to the real data; the corresponding relative systematic error is estimated to be at most of $\pm 1\%$.
- Selection of the impact parameter of the π_{**} candidate relative to the $D(\pi_*)\ell^-$ vertex:
  this impact parameter was required to be smaller than 100 μm, which allowed the selection of about 82% of genuine π_{**} candidates. A variation of $\pm 10\%$ of the impact parameter resolution modified the relative efficiency by about $\pm 2.5\%$, the magnitude depending on the considered D decay channel. A similar uncertainty was also inferred by comparing, in $D^{*+}\ell^-$ real data and simulation, the effect of a cut on the impact parameter of the lepton relative to the $D^0\pi_*\ell^-$ vertex.

The overall systematic uncertainty due to the impact parameter resolution is given in Table 3.

The uncertainty due to the π_{**} momentum spectrum was evaluated by comparing the π_{**} selection efficiencies in simulated $D_J \to D\pi$ and $D\pi\pi$ decays: a relative difference of $\pm 1\%$ was observed.

Error source	$D^0 h\ell^-$	$D^0\pi\ell^-$	$D^0 K\ell^-$	$D^+\pi\ell^-$	$D^{*+}\pi\ell^-$
$b \to \ell$ decay model [13]	± 1.2	± 1.2	± 1.2	± 1.2	± 1.2
τ_B [17]	± 1.9	± 1.8	± 2.2	± 1.6	± 1.2
π_{**} momentum spectrum	± 1.0	± 1.0	± 1.0	± 1.0	± 1.0
$\tau, c \to \ell$ background	± 3.5	± 3.5	± 4.2	± 3.5	± 3.5
"hadronic" background	± 2.5	± 2.1	± 9.2	± 2.4	± 2.3
BR($D^0 \to K^-\pi^+$) [1]	± 2.3	± 2.3	± 2.3	–	± 2.3
BR($D^+ \to K^-\pi^+\pi^+$) [1]		–		± 6.7	–
BR($D^{*+} \to D^0\pi^+$) [1]		–		–	± 2.0
fake $D\ell$ backgrounds	± 5.4	± 5.4	± 5.4	± 7.2	± 7.1
MC statistics	± 2.0	± 2.0	± 2.3	± 2.6	± 1.7
track reconstruction	± 1.3	± 1.3	± 1.5	± 1.6	± 1.6
impact parameter resolution	± 3.2	± 3.1	± 3.7	± 3.7	± 2.8
mass resolution	± 1.2	± 1.1	± 1.4	± 1.1	± 1.1
VD requirement	± 3.3	± 3.2	± 3.9	± 3.2	± 3.3
D vertex selection		–		± 3.3	–
K (from D) identification	± 2.6	± 2.6	± 3.1	± 2.6	–
π_{**} (or K_{**}) identification	–	± 2.1	± 18.1	± 1.2	± 1.2
lepton identification	± 2.0	± 1.9	± 2.3	± 2.0	± 2.0
Total	± 9.9	± 9.9	± 22.9	± 13.3	± 10.6

Table 3: Relative systematic uncertainties (%) on the b semileptonic branching fractions into $D^{**}\ell^-\bar{\nu}_\ell$ final states ("right" sign only).

5.6 Results

From the previous study, the b semileptonic branching fraction can be computed in each $D\pi\ell^-$ or $D^0 K\ell^-$ final state. The corresponding results are reported in Table 4 which includes the statistical and systematic errors. The "right" sign values are in agreement with those measured by the ALEPH collaboration [2], except for the $D^0\pi^+\ell^- X$ channel where the DELPHI result is two standard deviations larger.

The "wrong" sign results are at less than 2 standard deviations from zero, thus $D\pi\pi$ final states will be neglected in the following. The $D^0 K\ell^-$ production rate is also found to be compatible with zero. Thus only $D\pi\ell^-$ final states will be considered in the following. As a further cross-check, Tables 5-6 present the b semileptonic branching fraction measurement for electrons and muons separately and for the various D decay channels.

Using the production fraction BR($b \to \bar{B}^0$) =BR($b \to B^-$) $= 0.395 \pm 0.014$ [17], the following branching fractions are measured:

$$\begin{aligned} \mathrm{BR}(\bar{B}^0 \to D^0\pi^+\ell^-\bar{\nu}_\ell) + \mathrm{BR}(\bar{B}^0 \to D^{*0}\pi^+\ell^-\bar{\nu}_\ell) &= (2.70 \pm 0.64\ (stat) \pm 0.28\ (syst))\% \\ \mathrm{BR}(B^- \to D^+\pi^-\ell^-\bar{\nu}_\ell) + \mathrm{BR}(B^- \to D^{*+}\pi^-\ell^-\bar{\nu}_\ell) &= (2.08 \pm 0.47\ (stat) \pm 0.20\ (syst))\% \ . \end{aligned}$$

BR($b \to D^{**}\ell^-\bar{\nu}_\ell$) ($\times 10^{-3}$)				
$D^0 h\ell^- X$	$D^0\pi\ell^- X$	$D^0 K\ell^- X$	$D^+\pi\ell^- X$	$D^{*+}\pi\ell^- X$
DELPHI "right" sign				
$11.6 \pm 2.4 \pm 1.1$	$10.7 \pm 2.5 \pm 1.1$	$1.0 \pm 1.1 \pm 0.2$	$4.9 \pm 1.8 \pm 0.7$	$4.8 \pm 0.9 \pm 0.5$
DELPHI "wrong" sign				
$1.9 \pm 1.4 \pm 0.4$	$2.3 \pm 1.5 \pm 0.4$	$-0.4 \pm 0.6 \pm 0.1$	$2.6 \pm 1.5 \pm 0.4$	$0.6 \pm 0.7 \pm 0.2$
ALEPH "right" sign				
–	$4.7 \pm 1.3 \pm 1.0$	$2.6 \pm 1.2 \pm 0.8$	$3.0 \pm 0.7 \pm 0.5$	$4.7 \pm 0.8 \pm 0.6$

Table 4: Semileptonic branching fractions BR($b \to D^{**}\ell^-\bar{\nu}_\ell$) measured in DELPHI for each $D\pi\ell^-$ or $D^0 K\ell^-$ final state. Similar results obtained in ALEPH are also presented [2]. The first errors are statistical and the second systematic. Note that D^0s from the $D^{*+} \to D^0\pi^+_*$ decay mode are removed from the $D^0\ell^-$ results, which still include D^0s from $D^{*0} \to D^0\pi^0$ (or γ) decays; results on D^+ also include $D^{*+} \to D^+\pi^0$ (or γ) decays.

BR($b \to D^{**}\ell^-\bar{\nu}_\ell$) ($\times 10^{-3}$)	$D^0 h^+\ell^- X$	$D^+\pi^-\ell^- X$	$D^{*+}\pi^-\ell^- X$
e	8.8 ± 3.0	5.3 ± 2.3	5.1 ± 1.2
μ	14.6 ± 3.4	4.5 ± 2.5	4.4 ± 1.2
Average	11.6 ± 2.4	4.9 ± 1.8	4.8 ± 0.9

Table 5: Semileptonic branching fraction for electrons and muons separately. Errors are statistical only.

BR($b \to D^{**}\ell^-\bar{\nu}_\ell$) ($\times 10^{-3}$)	$D^0 h^+\ell^- X$	$D^{*+}\pi^-\ell^- X$
$K\pi$	13.6 ± 2.6	5.5 ± 1.5
$K\pi\pi\pi$	9.8 ± 4.1	5.7 ± 1.8
$K\pi\pi^0$		3.9 ± 1.3
Average	11.6 ± 2.4	4.8 ± 0.9

Table 6: Semileptonic branching fraction for the different D decay channels. Errors are statistical only.

According to isospin conservation rules and assuming that only $D\pi$ and $D^*\pi$ final states contribute, the ratios between final states involving charged and neutral pions are predicted to be:

$$\frac{D^0\pi^+ + D^{*0}\pi^+}{D^+\pi^0 + D^{*+}\pi^0} = \frac{D^+\pi^- + D^{*+}\pi^-}{D^0\pi^0 + D^{*0}\pi^0} = 2\,, \tag{9}$$

allowing the following branching fractions to be inferred:

$$\mathrm{BR}(\bar{B}^0 \to D\pi\ell^-\bar{\nu}_\ell) + \mathrm{BR}(\bar{B}^0 \to D^*\pi\ell^-\bar{\nu}_\ell) = (4.05 \pm 0.96\ (stat) \pm 0.42\ (syst))\% \tag{10}$$

$$\mathrm{BR}(B^- \to D\pi\ell^-\bar{\nu}_\ell) + \mathrm{BR}(B^- \to D^*\pi\ell^-\bar{\nu}_\ell) = (3.12 \pm 0.71\ (stat) \pm 0.30\ (syst))\% \tag{11}$$

These values are in good agreement. Neglecting $D\pi\pi$ final states and using as a constraint the equality of equations (10) and (11), the overall B meson semileptonic branching fraction into any $D^{(*)}\pi$ final state can be obtained:

$$\mathrm{BR}(\bar{B} \to D\pi\ell^-\bar{\nu}_\ell) + \mathrm{BR}(\bar{B} \to D^*\pi\ell^-\bar{\nu}_\ell) = (3.40 \pm 0.52\ (stat) \pm 0.32\ (syst))\% \ .$$

Assuming that the isospin invariance used in equation (9) applies also to $D\pi$ and $D^*\pi$ separately, the following branching fractions are also inferred:

$$\begin{aligned} \mathrm{BR}(\bar{B} \to D\pi\ell^-\bar{\nu}_\ell) &= (1.54 \pm 0.61\ (stat + syst))\% \\ \mathrm{BR}(\bar{B} \to D^*\pi\ell^-\bar{\nu}_\ell) &= (1.86 \pm 0.38\ (stat + syst))\% \end{aligned}$$

with a correlation coefficient of -0.33 between the results.

6 Overall b decay rate into $D\ell^-\bar{\nu}_\ell X$ final states

In this section, a measurement of the semileptonic branching fractions $\mathrm{BR}(b \to D\ell^-X)$, where D stands for D^0, D^+ or D^{*+}, is presented. The method used is similar to that described in Section 5.4:

$$\mathrm{BR}(b \to D\ell^-X) = \frac{\epsilon_Z}{N_Z}\ \frac{1}{2R_b}\ \frac{N(D_{K\pi}\ell)}{2\ \epsilon_{D\ell}\ \eta_{D\ell}}\ \frac{1}{f'_{\mathrm{cor}}}\ \frac{1 - f_{\tau,c\to\ell}}{\mathrm{BR}_D}\ -\ \mathcal{F}'_{D^*}\ +\ \mathcal{F}_{Dh\ell} \qquad (12)$$

where $N(D_{K\pi}\ell) = N(D\ell^-) - N(D\ell^+)$ is the difference between the total number of $D\ell$ candidates quoted in Table 1, using only the $K\pi$ ($K\pi\pi$, $K\pi\pi_*$) decay mode in the D^0 (D^+, D^{*+}) analyses; $f'_{\mathrm{cor}} = f_{M_D}\ f_{\mathrm{VD}}\ f_{D\mathrm{vtx}}\ f_{K\mathrm{id}}$; $\mathcal{F}'_{D^*}$ is only used for the D^0 sample where a fraction of $(7.6 \pm 0.4\ (stat))\%$ of $D^{*+} \to D^0\pi^+_*$ decays is included.

According to the simulation, the reconstruction efficiency of $D\ell$ final states depends slightly on whether or not the D meson originates from a D^{**}. In the absence of D^{**}, the reconstruction times selection efficiency, $\epsilon_{D\ell}$, of Table 2 has to be multiplied by the factor $\eta_{D\ell} = 1.08 \pm 0.02$ (1.13 ± 0.02, 1.07 ± 0.02) for a D^0 (D^+, D^{*+}) final state. Thus the observed production fraction of $D\pi\ell^-$ and $D^0K\ell^-$ final states (denoted $Dh\ell^-$) has to be taken into account in equation (12) and the following factor is introduced:

$$\mathcal{F}_{Dh\ell} = \frac{\eta_{D\ell} - 1}{\eta_{D\ell}}\ \mathrm{BR}(b \to Dh\ell^-X)\ . \qquad (13)$$

The overall b semileptonic branching fractions are thus measured to be:

$$\begin{aligned} \mathrm{BR}(b \to D^0\ell^-\bar{\nu}_\ell X) &= (7.04 \pm 0.34\ (stat) \pm 0.36\ (syst.exp) \pm 0.17\ (\mathrm{BR}_D))\% \\ \mathrm{BR}(b \to D^+\ell^-\bar{\nu}_\ell X) &= (2.72 \pm 0.19\ (stat) \pm 0.16\ (syst.exp) \pm 0.18\ (\mathrm{BR}_D))\% \\ \mathrm{BR}(b \to D^{*+}\ell^-\bar{\nu}_\ell X) &= (2.75 \pm 0.17\ (stat) \pm 0.13\ (syst.exp) \pm 0.09\ (\mathrm{BR}_D))\% \end{aligned} \qquad (14)$$

where the $D^0\ell^-$ result includes also D^0 coming from D^{*0} and also (contrarily to Section 5) $D^{*+} \to D^0\pi^+_*$ decays, the $D^+\ell^-$ result includes also D^+ coming from $D^{*+} \to D^+\pi^0$ (or γ) decays and X means "anything" (possibly a hadron coming from a D^{**}). These results are compared in Table 7 with those measured by the OPAL collaboration [19]: the D^0 and D^{*+} values are in agreement whereas the D^+ results present a difference of two standard deviations. The systematics are detailed in Table 8.

The relative yield of $D^{*+}\pi\ell^-\bar{\nu}_\ell X$ over all $D^{*+}\ell^-\bar{\nu}_\ell X$ is a contribution to the systematic uncertainty of various measurements, particularly of V_{cb} [3,5,20]. From Table 4 and equations (9) and (14), the following ratio is obtained:

$$\frac{\mathrm{BR}(b \to D^{*+}\pi^-\ell^-\bar{\nu}_\ell X) + \mathrm{BR}(b \to D^{*+}\pi^0\ell^-\bar{\nu}_\ell X)}{\mathrm{BR}(b \to D^{*+}\ell^-\bar{\nu}_\ell X)} = 0.26 \pm 0.05\ (stat) \pm 0.02\ (syst)$$

which significantly improves on a previous DELPHI measurement [5].

$\mathrm{BR}(b \to D\ell^-\bar{\nu}_\ell X)$ (%)	$D^0\ell^-$	$D^+\ell^-$	$D^{*+}\ell^-$
DELPHI	$7.04 \pm 0.34 \pm 0.36 \pm 0.17$	$2.72 \pm 0.19 \pm 0.16 \pm 0.18$	$2.75 \pm 0.17 \pm 0.13 \pm 0.09$
OPAL	$6.55 \pm 0.36 \pm 0.44 \pm 0.15$	$2.02 \pm 0.22 \pm 0.13 \pm 0.14$	$2.86 \pm 0.18 \pm 0.21 \pm 0.09$

Table 7: Overall semileptonic branching fractions into $D\ell^-$ final states as measured in DELPHI and OPAL [19]. The first errors are statistical, the second are experimental systematics and the last are due to the exclusive D branching fractions, BR_D.

Error source	$D^0\ell^-$	$D^+\ell^-$	$D^{*+}\ell^-$
$b \to \ell$ decay model [13]	± 1.2	± 1.2	± 1.2
τ_B [17]	± 0.2	± 0.2	± 0.2
$\tau, c \to \ell$ background	± 1.8	± 1.8	± 1.8
$\mathrm{BR}(D^0 \to K^-\pi^+)$ [1]	± 2.3	–	± 2.3
$\mathrm{BR}(D^+ \to K^-\pi^+\pi^+)$ [1]	–	± 6.7	–
$\mathrm{BR}(D^{*+} \to D^0\pi^+)$ [1]	–	–	± 2.0
MC statistics	± 2.4	± 2.4	± 2.7
track reconstruction	± 0.9	± 1.2	± 1.2
mass resolution	± 1.1	± 1.0	± 1.0
VD requirement	± 2.0	± 2.0	± 2.0
D vertex selection	–	± 3.1	–
K identification	± 2.4	± 2.4	–
lepton identification	± 1.8	± 1.8	± 1.8
Total	± 5.5	± 9.0	± 5.6

Table 8: Relative systematic uncertainties (%) on the b semileptonic branching fractions into $D\ell^-\bar{\nu}_\ell X$ final states.

7 Summary and conclusion

Using DELPHI data recorded from 1992 to 1995, the overall b semileptonic branching fractions into D^0, D^+ or D^{*+} final states have been obtained:

$$\begin{aligned}
\mathrm{BR}(b \to D^0\ell^-\bar{\nu}_\ell X) &= (7.04 \pm 0.34\ (stat) \pm 0.36\ (syst.exp) \pm 0.17\ (\mathrm{BR}_D))\% \\
\mathrm{BR}(b \to D^+\ell^-\bar{\nu}_\ell X) &= (2.72 \pm 0.19\ (stat) \pm 0.16\ (syst.exp) \pm 0.18\ (\mathrm{BR}_D))\% \\
\mathrm{BR}(b \to D^{*+}\ell^-\bar{\nu}_\ell X) &= (2.75 \pm 0.17\ (stat) \pm 0.13\ (syst.exp) \pm 0.09\ (\mathrm{BR}_D))\%
\end{aligned}$$

where the D^0 and D^+ results include also contributions from D^{*0} and D^{*+} decays.

Evaluating the yield of charged pions from higher excited states or from non-resonant $D^{(*)}\pi$ final states, the following branching fractions have been measured:

$$\begin{aligned}
\mathrm{BR}(b \to D^0\pi^+\ell^-\bar{\nu}_\ell X) &= (10.7 \pm 2.5\ (stat) \pm 1.1\ (syst))10^{-3} \\
\mathrm{BR}(b \to D^+\pi^-\ell^-\bar{\nu}_\ell X) &= (4.9 \pm 1.8\ (stat) \pm 0.7\ (syst))10^{-3} \\
\mathrm{BR}(b \to D^{*+}\pi^-\ell^-\bar{\nu}_\ell X) &= (4.8 \pm 0.9\ (stat) \pm 0.5\ (syst))10^{-3}
\end{aligned}$$

and

$$\begin{aligned}
\mathrm{BR}(b \to D^0\pi^-\ell^-\bar{\nu}_\ell X) &= (2.3 \pm 1.5\ (stat) \pm 0.4\ (syst))10^{-3} \\
\mathrm{BR}(b \to D^+\pi^+\ell^-\bar{\nu}_\ell X) &= (2.6 \pm 1.5\ (stat) \pm 0.4\ (syst))10^{-3} \\
\mathrm{BR}(b \to D^{*+}\pi^+\ell^-\bar{\nu}_\ell X) &= (0.6 \pm 0.7\ (stat) \pm 0.2\ (syst))10^{-3}
\end{aligned}$$

where the $D^{*+} \to D^0\pi^+_*$ decay mode is not included in the $\mathrm{BR}(b \to D^0\pi^\pm\ell^-\bar{\nu}_\ell X)$ results. Neglecting $D\pi\pi$ final states and assuming isospin invariance, the separated branching fractions are inferred:

$$\begin{aligned}
\mathrm{BR}(\bar{B} \to D\pi\ell^-\bar{\nu}_\ell) &= (1.54 \pm 0.61\ (stat + syst))\% \\
\mathrm{BR}(\bar{B} \to D^*\pi\ell^-\bar{\nu}_\ell) &= (1.86 \pm 0.38\ (stat + syst))\% \ .
\end{aligned}$$

The measured overall branching fraction:

$$\mathrm{BR}(\bar{B} \to D\pi\ell^-\bar{\nu}_\ell) + \mathrm{BR}(\bar{B} \to D^*\pi\ell^-\bar{\nu}_\ell) = (3.40 \pm 0.52\ (stat) \pm 0.32\ (syst))\%$$

is found, in good agreement with the expectation from the difference [1]:

$$\mathrm{BR}(\bar{B} \to \ell^-\bar{\nu}_\ell X) - \mathrm{BR}(\bar{B}^0 \to D^+\ell^-\bar{\nu}_\ell) - \mathrm{BR}(\bar{B}^0 \to D^{*+}\ell^-\bar{\nu}_\ell) = (3.85 \pm 0.42)\%$$

but is larger than a previous ALEPH result of $\mathrm{BR}(\bar{B} \to D\pi\ell^-\bar{\nu}_\ell) + \mathrm{BR}(\bar{B} \to D^*\pi\ell^-\bar{\nu}_\ell) = (2.26 \pm 0.29\ (stat) \pm 0.33\ (syst))\%$ [2].

Acknowledgements

We are greatly indebted to our technical collaborators, to the members of the CERN-SL Division for the excellent performance of the LEP collider, and to the funding agencies for their support in building and operating the DELPHI detector.
We acknowledge in particular the support of
Austrian Federal Ministry of Science and Traffics, GZ 616.364/2-III/2a/98,
FNRS–FWO, Belgium,
FINEP, CNPq, CAPES, FUJB and FAPERJ, Brazil,
Czech Ministry of Industry and Trade, GA CR 202/96/0450 and GA AVCR A1010521,
Danish Natural Research Council,
Commission of the European Communities (DG XII),
Direction des Sciences de la Matière, CEA, France,
Bundesministerium für Bildung, Wissenschaft, Forschung und Technologie, Germany,
General Secretariat for Research and Technology, Greece,
National Science Foundation (NWO) and Foundation for Research on Matter (FOM), The Netherlands,
Norwegian Research Council,
State Committee for Scientific Research, Poland, 2P03B06015, 2P03B1116 and SPUB/P03/178/98,
JNICT–Junta Nacional de Investigação Científica e Tecnológica, Portugal,
Vedecka grantova agentura MS SR, Slovakia, Nr. 95/5195/134,
Ministry of Science and Technology of the Republic of Slovenia,
CICYT, Spain, AEN96–1661 and AEN96-1681,
The Swedish Natural Science Research Council,
Particle Physics and Astronomy Research Council, UK,
Department of Energy, USA, DE–FG02–94ER40817.

References

[1] Review of Particle Physics, Eur. Phys. J. **C3** (1998) 1.

[2] ALEPH collab., D. Buskulic *et al.*, Zeit. Phys. **C73** (1997) 601.

[3] The LEP Heavy Flavour Steering Group, see http://www.cern.ch/LEPHFS/ and references therein.

[4] ALEPH collab., D. Buskulic *et al.*, Phys. Lett. **B345** (1994) 103.

[5] DELPHI collab., P. Abreu *et al.*, Zeit. Phys. **C71** (1996) 539.

[6] DELPHI collab., P. Aarnio *et al.*, Nucl. Instr. & Meth. **A303** (1991) 233.

[7] DELPHI collab., P. Abreu *et al.*, Nucl. Instr. & Meth. **A378** (1996) 57.

[8] V. Chabaud *et al.*, Nucl. Instr. & Meth. **A368** (1996) 314.

[9] DELPHI collab., P. Abreu *et al.*, Eur. Phys. J. **C9** (1999) 367.

[10] T. Sjöstrand, Comp. Phys. Comm. **82** (1994) 74.

[11] G. Borisov and C. Mariotti, Nucl. Instr. & Meth. **A372** (1996) 181.

[12] DELPHI collab., P. Abreu *et al.*, "Determination of $P(c \to D^{*+})$ and BR$(c \to \ell^+)$ at LEP 1", CERN-EP/99-67 (1999), submitted to Eur. Phys. J. C.

[13] The LEP Collaborations, ALEPH, DELPHI, L3, OPAL, the LEP Electroweak Working Group and the SLD Heavy Flavour and Electroweak Working Groups, "A Combination of Preliminary Electroweak Measurements and Constraints on the Standard Model", preprint CERN-EP/99-15, Geneva 1999.

[14] The LEP Heavy Flavour Working Group, "Input Parameters for the LEP/SLD Electroweak Heavy Flavour Results for Summer 1998 Conferences", LEPHF/98-01, http://www.cern.ch/LEPEWWG/heavy/lephf9801.ps.gz .

[15] DELPHI collab., P. Abreu *et al.*, "Measurements of the Z partial Decay Width into $c\bar{c}$ and Multiplicity of Charm Quarks per b Decay", CERN-EP/99-66 (1999), submitted to Eur. Phys. J. C.

[16] DELPHI collab., P. Abreu *et al.*, Phys. Lett. **B425** (1998) 399.

[17] The LEP B oscillations working group, "Combined Results on B^0 Oscillations: Results from Winter 1999 Conferences", LEPBOSC 99/1 (June 1999), http://www.cern.ch/LEPBOSC/combined_results/may_1999/ .

[18] I. Bigi and P.J. Dornan, Phys. Rept. **289** (1997) 1;
M. Neubert, CERN-TH/98-2 (1998), invited talk at the International Europhysics Conference on High Energy Physics (HEP 97), Jerusalem, Israel (19-26 Aug 1997), ed. D. Lellouch, G. Mikenberg, E. Rabinovici (Springer, 1998).

[19] OPAL collab., R. Akers *et al.*, Zeit. Phys. **C67** (1995) 57.

[20] OPAL collab., K. Ackerstaff *et al.*, Phys. Lett. **B395** (1997) 128;
ALEPH collab., D. Buskulic *et al.*, Phys. Lett. **B395** (1997) 373.

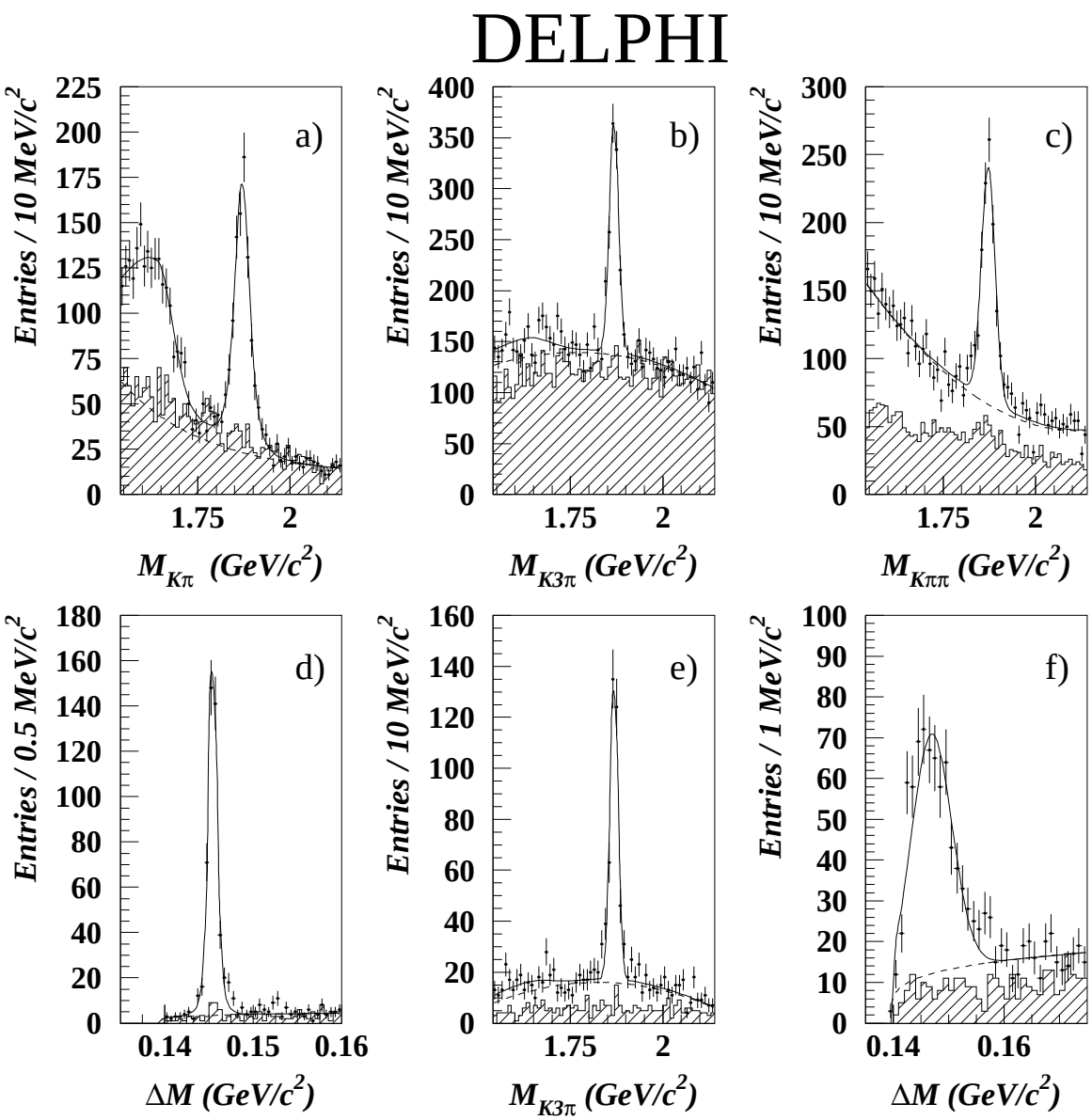

Figure 1: Invariant mass distributions in the (a) $D^0 \to K^-\pi^+$ (b) $D^0 \to K^-\pi^+\pi^+\pi^-$ (c) $D^+ \to K^-\pi^+\pi^+$ and (e) $D^{*+} \to (K^-\pi^+\pi^+\pi^-)\pi^+_*$ decay channels; mass difference distributions $M(K^-\pi^+\pi^+_*) - M(K^-\pi^+)$ in the (d) $D^{*+} \to (K^-\pi^+)\pi^+_*$ and (f) $D^{*+} \to (K^-\pi^+(\pi^0))\pi^+_*$ decay channels. The reconstructed D^{*+} candidates have been removed in a,b,c. Right charge $D\ell^-$ (dots) and wrong charge $D\ell^+$ (hatched histogram) events are shown. The solid line curves are fits which include a background parameterisation (dashed curve alone) and Gaussian functions for the signal (see Section 4).

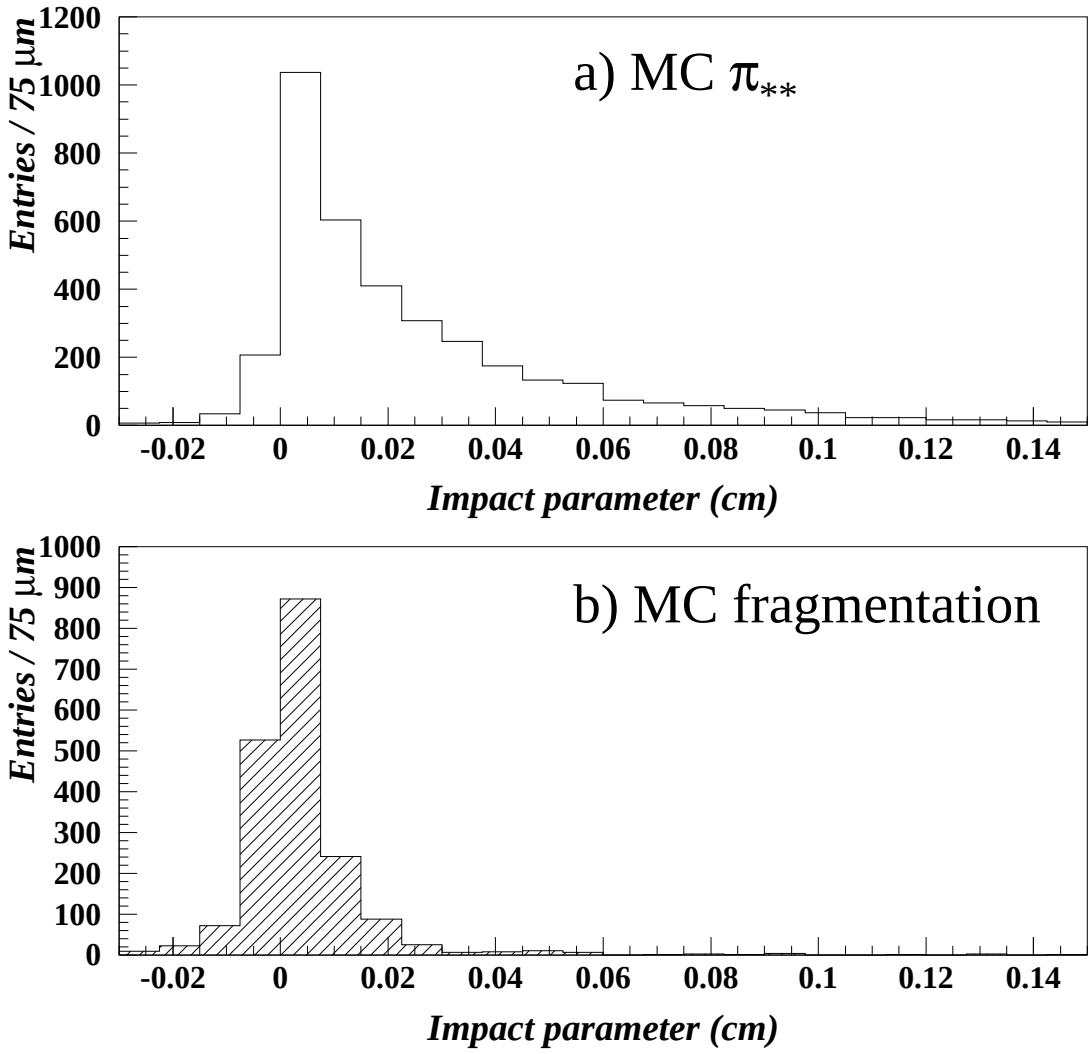

Figure 2: Impact parameter relative to the primary interaction vertex in simulated B semileptonic decays for a) π_{**} from D^{**} decay (using a B mean lifetime value of 1.6 ps) and b) charged particles from jet fragmentation (see Section 5.1).

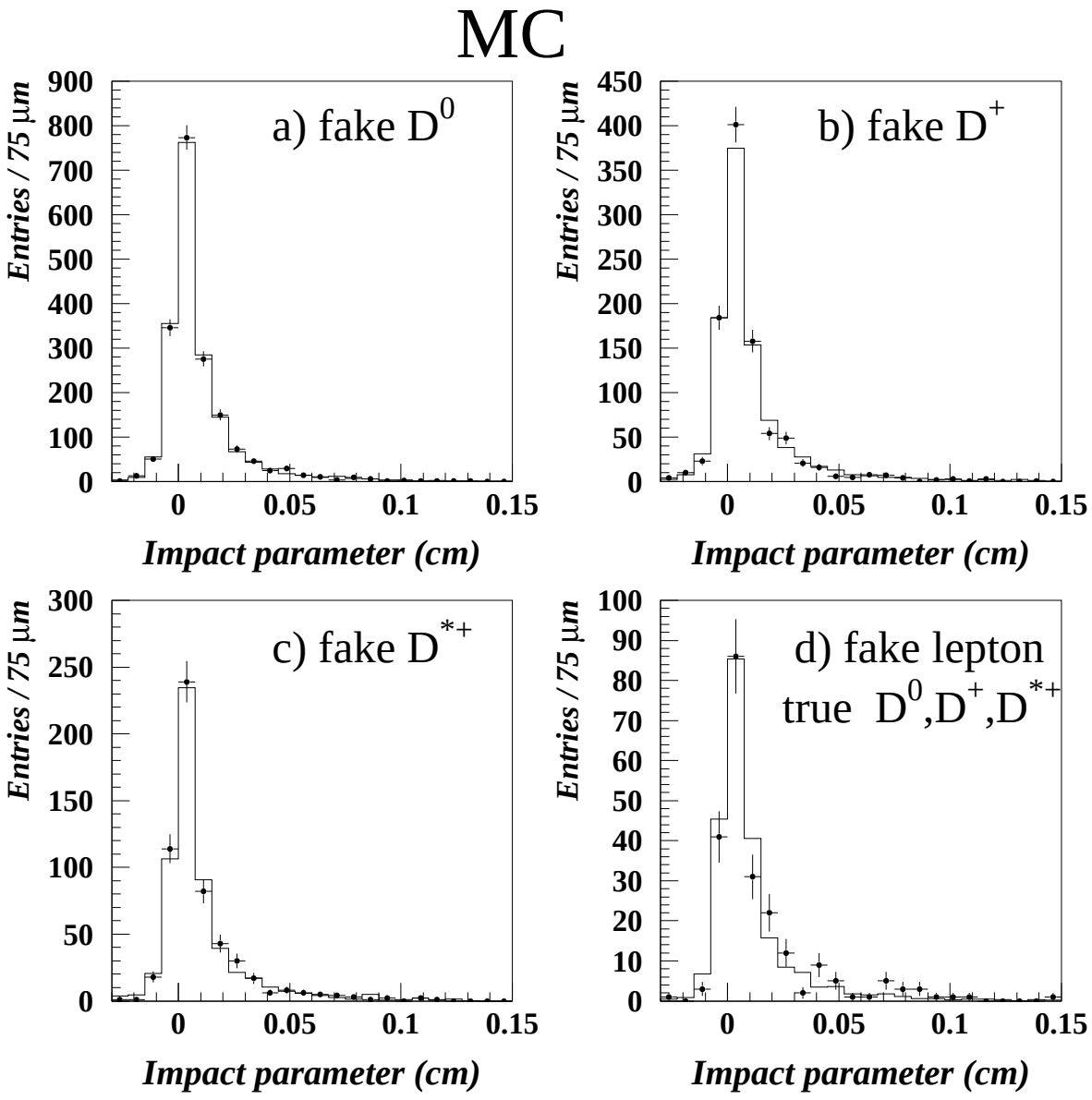

Figure 3: In the simulation: impact parameter distributions of pions accompanying (a-c) a fake D meson (points with error bars) or a D selected in the tails of the mass distributions (histograms); (d) a fake lepton (points with error bars) or a $D\ell^+$ where the D was selected in the signal region (histograms, see Section 5.2).

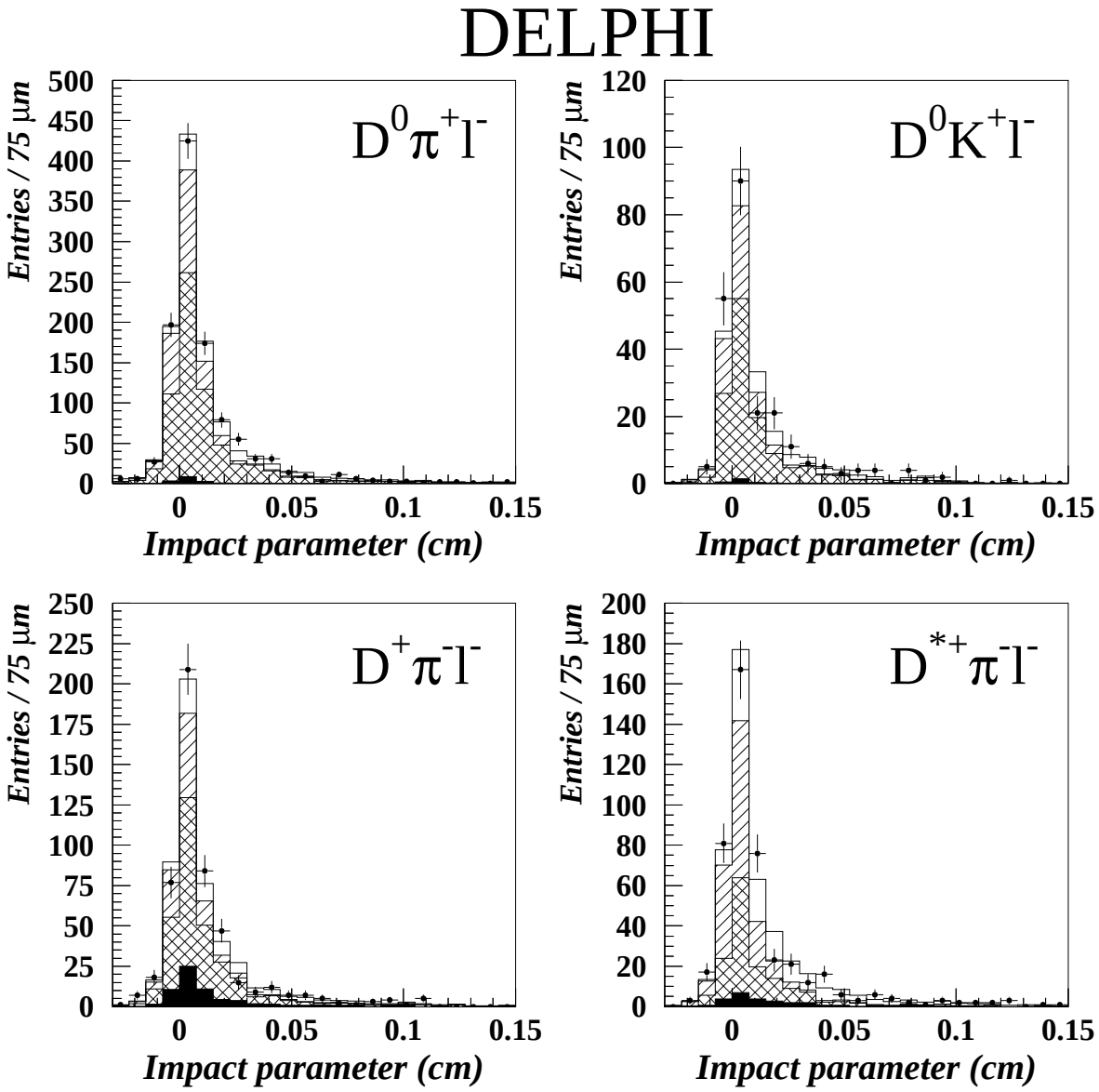

Figure 4: Impact parameter relative to the primary interaction vertex in real data for "right" sign $D^0\pi^+$, D^0K^+, $D^+\pi^-$ and $D^{*+}\pi^-$ candidates. The black and cross-hatched histograms are the estimated contributions from fake leptons and fake D mesons, respectively. The hatched and empty area histograms are the fitted contributions from jet fragmentation and π_{**} from D^{**} decays, respectively (see Section 5.3).

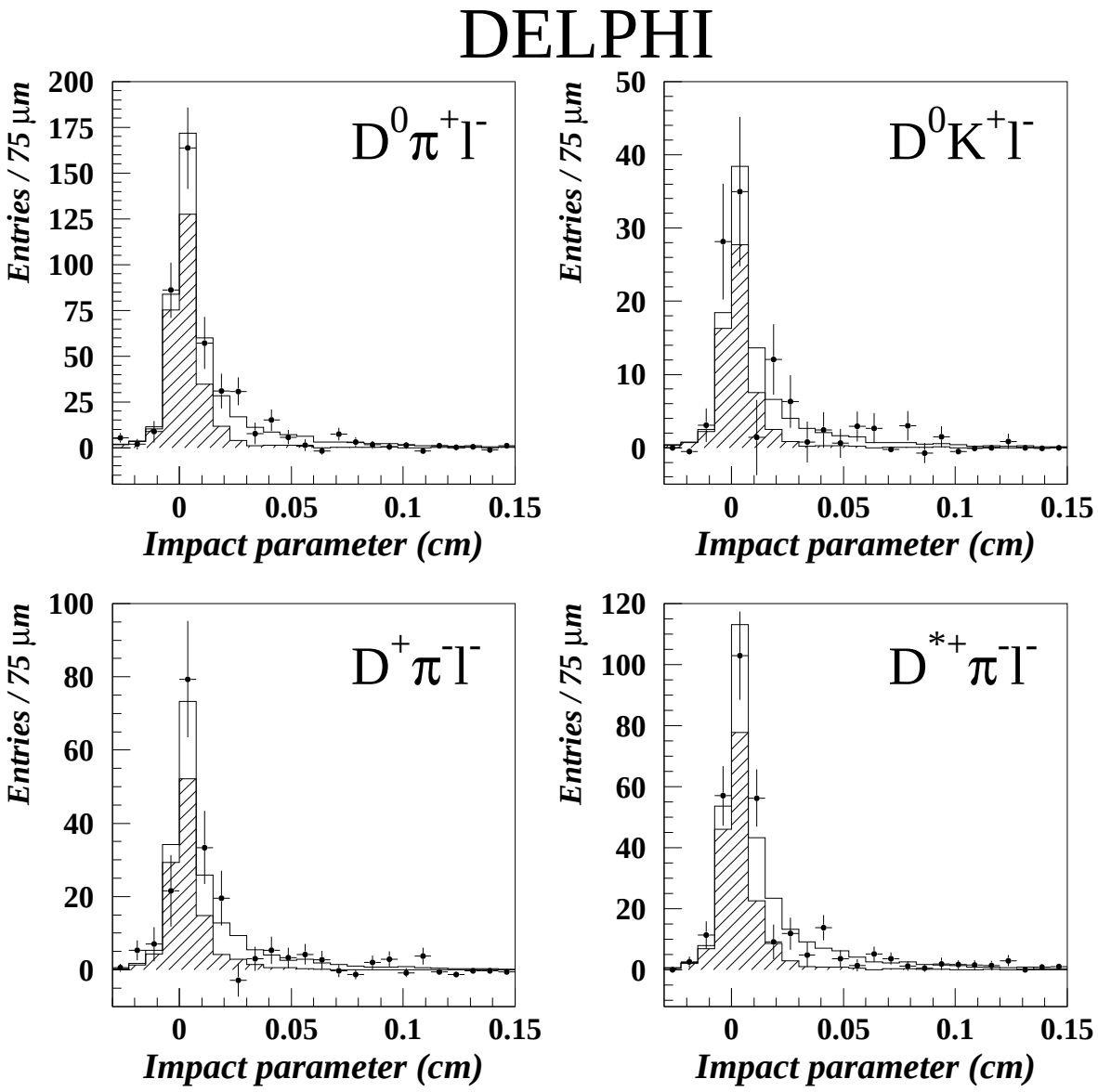

Figure 5: Impact parameter relative to the primary interaction vertex in real data for background subtracted "right" sign $D^0\pi^+$, D^0K^+, $D^+\pi^-$ and $D^{*+}\pi^-$ candidates. The hatched and empty area histograms are the fitted contributions from jet fragmentation and π_{**} from D^{**} decays, respectively (see Section 5.3).

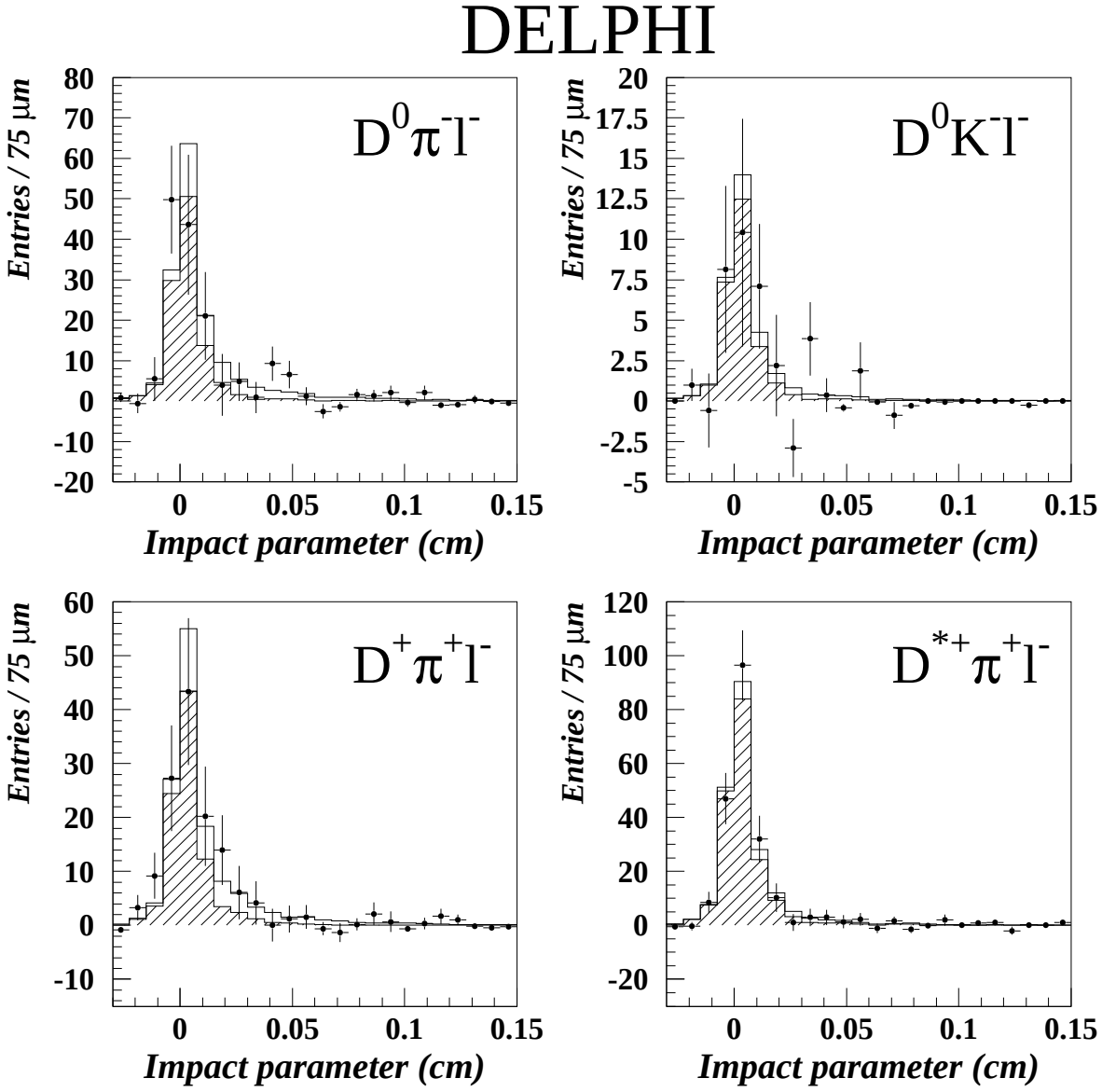

Figure 6: Same as Figure 5 for background subtracted "wrong" sign $D^0\pi^-$, D^0K^-, $D^+\pi^+$ and $D^{*+}\pi^+$ candidates.